

**NO₂ long-range
transport events in
GOME-2 data**

A. W. Zien et al.

This discussion paper is/has been under review for the journal Atmospheric Chemistry and Physics (ACP). Please refer to the corresponding final paper in ACP if available.

Systematic analysis of tropospheric NO₂ long-range transport events detected in GOME-2 satellite data

A. W. Zien, A. Richter, A. Hilboll, A.-M. Blechschmidt, and J. P. Burrows

Institute for Environmental Physics, University of Bremen, Bremen, Germany

Received: 19 October 2013 – Accepted: 12 November 2013 – Published: 27 November 2013

Correspondence to: A. W. Zien (achim.zien@iup.physik.uni-bremen.de)

Published by Copernicus Publications on behalf of the European Geosciences Union.

Title Page

Abstract

Introduction

Conclusions

References

Tables

Figures

⏪

⏩

◀

▶

Back

Close

Full Screen / Esc

Printer-friendly Version

Interactive Discussion



Abstract

Intercontinental long-range transport (LRT) events of NO₂ relocate the effects of air pollution from emission regions to remote, pristine regions. We detect transported plumes in tropospheric NO₂ columns measured by the GOME-2/MetOp-A instrument with a specialized algorithm and trace the plumes to their sources using the HYSPLIT Lagrangian transport model. With this algorithm we find 3808 LRT events over the ocean for the period 2007 to 2011. LRT events occur frequently in the mid-latitudes, emerging usually from coastal high-emission regions. In the free troposphere, plumes of NO₂ can travel for several days to the polar oceanic atmosphere or to other continents. They travel along characteristic routes and originate from both continuous anthropogenic emission and emission events such as bush fires. Most NO₂ LRT events occur during autumn and winter months, when meteorological conditions and emissions are most favorable. The evaluation of meteorological data shows that the observed NO₂ LRT is often linked to cyclones passing over an emission region.

1 Introduction

The transport of atmospheric pollution over long distances mostly affects long-lived species, such as CO, SO₂ and O₃. During long-range transport (LRT) of chemical species, trace gases are transported over intercontinental distances, relocating gases from emission to remote and pristine regions. As a result, air pollution has to be regarded as a global instead of a local phenomenon. Under certain conditions, this can also affect short-lived species which are commonly considered to be bounded to their emission regions.

While long-lived gas species can also mix slowly in the atmosphere to reach remote regions, a short-lived species has to travel fast before it is eventually converted into other species.

NO₂ long-range transport events in GOME-2 data

A. W. Zien et al.

Title Page

Abstract

Introduction

Conclusions

References

Tables

Figures



Back

Close

Full Screen / Esc

Printer-friendly Version

Interactive Discussion



**NO₂ long-range
transport events in
GOME-2 data**

A. W. Zien et al.

Title Page

Abstract

Introduction

Conclusions

References

Tables

Figures

◀

▶

◀

▶

Back

Close

Full Screen / Esc

Printer-friendly Version

Interactive Discussion



Here, we investigate the long-range transport of NO₂. Its lifetime in the planetary boundary layer (PBL) amounts to a few hours, depending on the strength of solar irradiation and on the available radical species. This, combined with low wind speeds near the surface, makes long-range transport of anthropogenic NO₂ in the planetary boundary layer very unlikely.

Still, satellite observations of NO₂ frequently exhibit such long-range transport events and allow a systematic analysis of their properties – such as their NO₂ content, altitude and age.

NO₂ is a toxic trace gas. A major fraction of the emissions takes place in the form of NO which then rapidly converts to NO₂ until the Leighton photostationary state is achieved at a ratio of NO/NO_x ≈ 0.2–0.8 (Ehhalt et al., 1992) – depending on radiative flux, available radical species and air pressure. NO_x is defined as the sum of the species NO and NO₂.

NO and NO₂ emissions originate from various sources. The dominant sources are anthropogenic emissions from combustion processes in transportation, industry and agricultural biomass burning, as well as natural sources such as lightning emissions, natural biomass burning and microbial soil emissions. Martin et al. (2003) report a total yearly NO_x emission rate of 43 Tg Na⁻¹ in 1996–1997, with anthropogenic sources contributing roughly half of the emissions.

NO₂ harms respiratory organs. It also reacts with OH to form HNO₃ which permanently removes the NO₂ from the air masses and results in acid rain. Besides that, NO₂ directly impacts the ozone cycle in the troposphere, where it favors O₃ production. The presence of OH and volatile organic compounds (VOCs) can amplify this effect.

The lifetime of NO₂ ranges from around 8 h in a typical planetary boundary layer scenario to a few days in the upper troposphere (Ehhalt et al., 1992; Beirle et al., 2011).

A long-range transport (LRT) event denotes a distinct plume of trace gas being exported from an emission region to a downwind region over a long distance, typically several thousand kilometers. While long-range transport could, in principle, take place

in the boundary layer, it is more likely that the actual transport happens after convection out of the planetary boundary layer into the free troposphere, where wind speeds are much higher, due to a lack of interaction with the surface.

For NO₂, long-range transport will predominantly take place in the free troposphere, where – in addition to the higher windspeed – its lifetime is extended to up to four days, due to lower concentrations of radical species. As NO₂ is mainly emitted in the boundary layer, this phenomenon could be expected to be rare. For it to occur, there has to be a mechanism to lift polluted air-masses into the free troposphere.

Once this happens, the NO₂ is transported from emission regions to remote, pristine regions, e.g. over the oceans, into polar regions or to other continents. This means that the NO₂ in these cases does not only affect its source region, but has regional or even global impacts.

As this study will show, NO₂ long-range transport plumes can have a horizontal extent of more than 1000 km. Due to this large extent, plumes are subject to horizontal shear winds. This results in filamentation and typical arc-like structures after a few days. The plume will also disperse over the course of the transport, typically after a few days (Rastigejev et al., 2010).

Due to chemical conversion and physical dispersion and filamentation, intercontinental NO₂ long-range transport events are usually seen departing from an emission region to the ocean, but they dissolve before arriving on another continent. Over the course of transport, NO₂ partly is converted into peroxyacyl nitrate (PAN) and other reservoir species, which may then release upon descent over the shore, when concentrations of radical species, pressure and temperature increase (Singh and Hanst, 1981; Schultz et al., 1998; Walker et al., 2010). This leads to an effective relocation of NO_x emissions.

NO₂ concentrations are observed both via in-situ and remote sensing methods. As long-range transport is a large-scale phenomenon, we use data from satellite remote sensing observations for our large-scale and global analysis.

NO₂ long-range transport events in GOME-2 data

A. W. Zien et al.

Title Page

Abstract

Introduction

Conclusions

References

Tables

Figures

◀

▶

◀

▶

Back

Close

Full Screen / Esc

Printer-friendly Version

Interactive Discussion



NO₂ long-range transport events in GOME-2 data

A. W. Zien et al.

Title Page

Abstract

Introduction

Conclusions

References

Tables

Figures

◀

▶

◀

▶

Back

Close

Full Screen / Esc

Printer-friendly Version

Interactive Discussion



However, NO₂ long-range transport events are rarely seen in common satellite data. This can lead to the false assumption that they also occur rarely. The reason for this lies in the common practice of filtering cloudy pixels from satellite observations. This is done because clouds complicate the radiative transfer and make the retrieval of trace gas concentrations harder. In particular, the sensitivity to NO₂ in the boundary layer is reduced in presence of clouds for most common observation scenarios.

If we omit the cloud filter, we observe many long-range transport events just by browsing through the data. Due to their rapid movement, such events can only be seen in daily or orbit-wise data – not in data averaged over longer time periods.

For different chemical species, long-range transport events have received more attention in the last few years. The Hemispheric Transport of Air Pollutants (HTAP) task force was created to collect data and knowledge on this phenomenon and assess its impact on the environment. In their report (Dentener et al., 2010), they find that a significant fraction of ozone pollution in the Northern Hemisphere is driven by transport from remote sources, mostly of ozone precursors such as methane and NO₂. They expect the resulting increased base levels of ozone to lead to an increased threat to human health and crop yields.

There are a number of satellite based case studies of individual events of NO₂ long-range transport. Wenig et al. (2003) report the first observation of such an event, a plume emitted from South Africa in May 1998. In their study, a high-pressure system favored a localized build-up of NO₂ concentrations which were then rapidly lifted to an altitude of 2–6 km above mean sea level (a.m.s.l.) by a passing low-pressure system. There, longer lifetime and higher wind speeds allowed the NO₂ to travel onto the open ocean.

Stohl et al. (2003) investigated an episode in which an explosively developing cyclone transported a significant plume of NO₂ over the Atlantic in about one day. The NO₂ was lifted upwards by a warm conveyor belt (WCB). In a climatological study, they find intercontinental express highways between North America and Europe which are

much stronger in winter and can contribute about 2–3 pptv of European NO₂ concentrations during winter.

Schaub et al. (2005) discuss an event during which NO₂ from the central German Ruhr area was lifted into the free troposphere (over the course of a day) and transported into the Alps where a significant increase in concentrations was measured in-situ on the Zugspitze and on multiple sites in Switzerland.

Studies by Spichtinger et al. (2001) and Riuttanen et al. (2013) illustrate further aspects of individual, observed transport events.

Unfortunately, there are – to our knowledge – no in-situ measurements of tropospheric NO₂ long-range transports by aircraft which would allow us to determine typical vertical concentration profiles and verify the results of this study with non-satellite observations.

Lin et al. (2010) have focussed on modeling NO₂ long-range transport with global chemical transport models (GCTMs). They find that 8–15% of NO_x emissions are transported over 1000 km from their source regions, using WRF-Chem and CMAQ for rapid vertical transport and MOZART as GCTM. They also note that in most GCTMs, rapid convection (such as in frontal passages) is not adequately represented, which biases the simulation of long-range transport events. The modeling of horizontal transport tends to dilute the plumes' boundaries, which are found to be rather sharp in observational data.

So far there has – to our knowledge – not been a systematic study of NO₂ long-range transport events using observational data. Such studies are necessary in order to judge the impact of NO₂ long-range transport on the atmospheric chemistry in pristine and sensitive environments such as the Arctic and to validate its impact as estimated from GCTMs.

In this study, we have used daily maps of tropospheric NO₂ from the GOME-2/MetOp-A instrument (Sect. 2). We implemented an algorithm to detect long-range transport events over the ocean in this timeseries of two-dimensional data (Sect. 3). This allows us to perform a systematic study of long-range transport of NO₂. We

NO₂ long-range transport events in GOME-2 data

A. W. Zien et al.

Title Page

Abstract

Introduction

Conclusions

References

Tables

Figures

◀

▶

◀

▶

Back

Close

Full Screen / Esc

Printer-friendly Version

Interactive Discussion



NO₂ long-range transport events in GOME-2 data

A. W. Zien et al.

Title Page

Abstract

Introduction

Conclusions

References

Tables

Figures

◀

▶

◀

▶

Back

Close

Full Screen / Esc

Printer-friendly Version

Interactive Discussion



(and other features like the Ring-spectrum) are fitted in a suitable wavelength window. The low-variance part is approximated by a polynomial function. The remaining high-variance parts of the measured optical depth are fitted by reference spectra (from laboratory measurements) for the relevant trace gases in this regime. Given the absorption coefficient and employing the Beer–Lambert law, this yields the trace gas density integrated along the light path for the selected species.

This is a valid approximation as long as the absorption does not saturate. Typical optical thicknesses of NO₂ for polluted areas are on the order of up to 10⁻³, so that saturation does not impact observations.

Usually, the light-path is slanted and features single and multiple scattering on molecules, cloud droplets and aerosols in the atmosphere. The derived quantity is thus called the slant column density (SCD) and is measured in molecules cm⁻². It can be interpreted as:

$$\text{SCD}_{\text{NO}_2} = \frac{1}{I_{\text{total}}} \sum_i \int_{\text{sun}}^{\text{observer}} \rho_{\text{NO}_2}(s_i) I_i ds_i, \quad (1)$$

which averages the integrated NO₂ concentration $\rho_{\text{NO}_2}(s_i)$ along all lightpaths s_i (from the sun to the observer) with the respective contribution I_i of this light path to the total intensity I_{total} observed at the instrument ($I_{\text{total}} = \sum_i I_i$).

For this study, we use data from the Bremen GOME-2 slant column density product as described by Richter and Burrows (2002) and Richter et al. (2011), which includes an NO₂ fit in the wavelength range from 425–497 nm. We analyze data from 4 January 2007 to 31 December 2011.

For most purposes, our GOME-2 NO₂ product uses FRESCO+ (Wang et al., 2008) to determine the cloud fraction and excludes pixels with a cloud fraction of $\text{CF} \geq 0.2$. For the analysis of NO₂ long-range transport, no cloud-filtering was applied to the data, as opposed to common practice. A systematic study of this phenomenon requires us to include cloudy data in the study, as most transport events are associated with frontal

systems which are accompanied by clouds and these events would otherwise only be partly visible or entirely missing in the data.

After the trace gas retrieval we have obtained a 2-dimensional map of the global slant column density as it is observed over the Earth's surface, for each day. However, the slant column density alone is hard to interpret. Therefore, we convert the slant column density to the vertical column density (VCD), which is independent of the light path and is a measure of the trace gas concentration integrated vertically from the surface of the Earth to the top of the atmosphere (ToA):

$$\text{VCD}_{\text{NO}_2} = \int_{\text{surface}}^{\text{ToA}} \rho_{\text{NO}_2}(h) dh. \quad (2)$$

In this study, we are interested in the tropospheric NO_2 distribution only, so we apply a stratospheric correction, removing any stratospheric contributions. Here, the stratospheric part of the measured NO_2 column is estimated from a 3-D chemical transport model (CTM), the B3dCTM (Aschmann et al., 2009; Hilboll et al., 2013). The obtained stratospheric NO_2 is offset to represent the zonally averaged NO_2 in the reference sector (Richter and Burrows, 2002): a strip over the remote Pacific – between 180 and 140°W – which is assumed to not contain any tropospheric NO_2 . This is then converted to a stratospheric slant column density map (via a stratospheric air-mass factor, see below) and subsequently subtracted from the total slant column density map to produce the tropospheric slant column density map.

This value contains no information about the altitude of the measured trace gas. To estimate the NO_2 pollution in a pixel, we need to model the lightpath and apply a corresponding correction – called the air-mass factor (AMF) – to obtain the vertical column density.

$$\text{VCD} = \frac{\text{SCD}}{\text{AMF}} \quad (3)$$

NO₂ long-range transport events in GOME-2 data

A. W. Zien et al.

Title Page

Abstract

Introduction

Conclusions

References

Tables

Figures

◀

▶

◀

▶

Back

Close

Full Screen / Esc

Printer-friendly Version

Interactive Discussion



The air-mass factor for a scene is derived from radiative transfer models initialized with a suitable scenario.

As typical NO₂ long-range transport events extend over hundreds of kilometers, we grid the retrieved data onto a grid with a cell size of 0.5° × 0.5° – to speed up computing times and reduce retrieval uncertainties – without significantly impacting our results.

2.1 Vertical column densities (VCDs) in partially cloudy scenes

To convert the NO₂ slant-column densities into vertical-column densities, we need to determine the air-mass factor, which interrelates these two. The air-mass factor describes, by which factor the vertical column density differs from the slant column density due to the radiative transfer (RT) from light source to observer.

We refrain from using a cloud-filter which removes satellite observations that show a certain degree of cloudiness. Long-range transport events are commonly linked to frontal systems and thus to cloud formation. In order to observe these events, we need to take cloudy pixels into account (see Fig. 1).

For cloud-free scenes, usually a climatology of NO₂ vertical profiles is used to determine the air-mass factor under various geometric configurations via radiative transfer simulations. Here, we use the SCIATRAN 3.1 radiative transfer model (Rozanov et al., 2005, 2013) to perform air-mass factor calculations.

For cloudy scenes this approach is not sufficient. The cloud drastically impacts the radiative transfer and may have varying influence on the air-mass factor, depending on the relation between the vertical profile of the NO₂ and the cloud. Especially, the so-called block air-mass factor (BAMF) is altered. The block air-mass factor denotes the sensitivity of the observations to a trace gas at a given altitude (Palmer et al., 2001). It can be visualized as the mean factor of light-path enhancement at a specific altitude. Neglecting saturation effects, the block air-mass factor relates to the air-mass factor

NO₂ long-range transport events in GOME-2 data

A. W. Zien et al.

[Title Page](#)[Abstract](#)[Introduction](#)[Conclusions](#)[References](#)[Tables](#)[Figures](#)[◀](#)[▶](#)[◀](#)[▶](#)[Back](#)[Close](#)[Full Screen / Esc](#)[Printer-friendly Version](#)[Interactive Discussion](#)

as:

$$AMF = \frac{\int_{\text{surface}}^{\text{ToA}} BAMF(h)\rho(h)dh}{\int_{\text{surface}}^{\text{ToA}} \rho(h)dh} \quad (4)$$

Clouds alter the block air-mass factor in multiple ways. The exact behavior depends on geometry and cloud properties. Typical effects are (Hild et al., 2002; Eskes and Boersma, 2003):

- The cloud provides a surface of high reflectivity. The block air-mass factor is enhanced close over the cloud top (albedo effect).
- Inside the cloud, multiple scattering takes place which elongates the mean light path and leads to a further increased block air-mass factor in the top layers. Less light penetrates into the lower layers, which in turn rapidly decreases the block air-mass factor towards the cloud bottom (multiple scattering effect).
- Little light penetrates to the atmosphere below the cloud and even less gets transmitted again to the satellite, which leads to a relatively small and stable block air-mass factor for the atmosphere between surface and cloud (shielding effect).

These effects are illustrated in Fig. 2.

Further interesting effects can occur when clouds reside over bright surfaces (snow and ice). Due to the high reflectivity of the surface, not much light is absorbed there. Instead, light between the surface and the cloud bottom will continually propagate back and forth until it finally penetrates the cloud and reaches the instrument. This leads to a vastly increased light-path and can lead to an increased block air-mass factor below the cloud due to the cloud's presence.

This effect is hard to find in satellite data, as typical observation geometries over bright scenes allow only for a mitigation of the shielding effect, not an absolute enhancement of the air-mass factor. It may, however, lead to an overestimation of NO₂ content when plumes are observed over sea-ice.

NO₂ long-range transport events in GOME-2 data

A. W. Zien et al.

Title Page

Abstract

Introduction

Conclusions

References

Tables

Figures

◀

▶

◀

▶

Back

Close

Full Screen / Esc

Printer-friendly Version

Interactive Discussion



NO₂ long-range transport events in GOME-2 data

A. W. Zien et al.

Title Page

Abstract

Introduction

Conclusions

References

Tables

Figures

◀

▶

◀

▶

Back

Close

Full Screen / Esc

Printer-friendly Version

Interactive Discussion



To take the effect of clouds on the radiative transfer into account, we first divide each satellite pixel into a cloudy and a cloud-free fraction, thus obtaining a geometric cloud fraction (CF). We obtain this cloud fraction by modeling the reflectivity of the pixel both under clear conditions and under cloudy conditions (with assumed cloud properties).

5 The reflectivity R is derived from nadir measurements and solar irradiance as

$$R(437.5\text{ nm}) = \frac{I_{\text{nadir}}(437.5\text{ nm})}{I_0(437.5\text{ nm})}. \quad (5)$$

Then, the cloud fraction is obtained by modelling the observed reflectivity from the combined reflectivity of cloudy and clear part, similar to the method described in Wang et al. (2008), but using directly the wavelength range in which we retrieve NO₂ optical depths.

10

$$\text{CF} = \frac{R_{\text{obs}} - R_{\text{cloud-free}}}{R_{\text{cloudy}} - R_{\text{cloud-free}}}. \quad (6)$$

This is a simple approach. It is quick and robust and operates directly in the wavelength we are interested in, 437.5 nm, where the most relevant absorption features are located. For this study, we use the monthly albedo climatologies based on MERIS data by Popp et al. (2011) to model cloudy and cloud-free reflectivities. Operationally, we obtain the reflectivity values from a look-up table.

15

However, this yields only the geometric cloud fraction. For purposes of determining the air-mass factor, we need to use the radiance cloud fraction: the fraction of the radiation entering the detector that was influenced by clouds. This is obtained by weighting the cloud fraction with the modeled reflectivities.

20

$$\text{CF}_{\text{radiance}} = \frac{\text{CF} R_{\text{cloudy}}}{\text{CF} R_{\text{cloudy}} + (1 - \text{CF}) R_{\text{cloud-free}}}. \quad (7)$$

Usually, this value will be larger than the geometric cloud fraction, because cloud reflectivities are higher than surface reflectivities for all but very white surfaces with an

albedo $\gtrsim 0.8$. This means, that even small cloud fractions have a strong impact on the air-mass factor.

Now, we determine the air-mass factor by weighting the cloudy and cloud-free air-mass factor by the radiance cloud fraction:

$$5 \quad \text{AMF}_{\text{total}} = \text{CF}_{\text{radiance}} \cdot \text{AMF}_{\text{cloudy}} + (1 - \text{CF}_{\text{radiance}}) \cdot \text{AMF}_{\text{cloud-free}} \quad (8)$$

Usually, the cloud-free air-mass factor is determined either from a standard atmospheric profile or from climatological simulations (like MOZART, Horowitz et al., 2003). These cannot, however, be used for analysis of long-range transport events, as the NO_2 will typically be strongly localized in altitude (Rastigejev et al., 2010) and deviate from stationary conditions.

The air-mass factor depends on where in vertical direction the trace gas is situated. This effect becomes stronger when there are clouds in the scene. However, the precise altitude is not needed, as long as we know the position of the trace gas with respect to the cloud (see Fig. 2 and Kokhanovsky and Rozanov, 2009).

15 Measurements from the TRACE-P campaign (Crawford et al., 2003) suggest that, for a long-range transport event associated with a cold front passing over an emission region, the trace gases (in their case CO) tend to be homogeneously mixed inside the cloud. It is possible that fractions of the trace gas content are also situated below or above the cloud due to the nature of convective processes, condensation and subsidence of liquid water droplets.

20 A detailed analysis of the air-mass factor's dependency on radiation geometry and surface properties for varying relative cloud and NO_2 profiles shows that if the NO_2 is well mixed inside the cloud, the errors of missing NO_2 slightly above or below the cloud are on the order of $\Delta\text{AMF}/\text{AMF} \lesssim 15\%$ (Fig. 3). This simplification holds, if most of the NO_2 is mixed inside the cloud.

25 If significant parts of the trace gas are situated above (or below) the cloud, we will underestimate (respectively overestimate) the air-mass factor. This effect is especially strong under non-nadir viewing and irradiation geometries. However, the effects of

NO_2 long-range transport events in GOME-2 data

A. W. Zien et al.

Title Page

Abstract

Introduction

Conclusions

References

Tables

Figures

◀

▶

◀

▶

Back

Close

Full Screen / Esc

Printer-friendly Version

Interactive Discussion



missing NO₂ above and below the cloud compensate each other for solar zenith angles of 40–70°, which is the range most relevant for NO₂ long-range transport.

Based on these sensitivity studies, an NO₂ block profile that is homogeneously mixed inside the cloud and zero elsewhere is selected as the modeling hypothesis for cloudy air-mass factors.

We assume a vertical block profile of NO₂ both for the cloudy and the clear sky case, where NO₂ is homogeneously distributed between 3–5 km a.g.l. and absent in all other parts of the atmosphere. If present, a cloud is assumed to extend over exactly the same altitude range. This approach is used for simplification and only valid for long-range transport processes. During such processes, the exact altitude of the NO₂ content has little impact on the resulting air-mass factor as long as any NO₂ will be mixed inside a cloud, if present.

A sensitivity study shows that from a broad sample of setups of surface and cloud properties, the 3–5 km a.g.l. scenario is situated right in the center of the resulting air-mass factors (deviating by less than 1% from the mean) over all occurring geometries (Fig. 5). The relative standard deviation of the resulting air-mass factors from the whole set of setups is less than 3% over all viewing geometries.

The estimated tropospheric NO₂ vertical column density (VCD) is finally calculated by applying the combined cloudy and cloud-free air-mass factor to the tropospheric NO₂ slant column density.

The NO₂ product described here is used only for long-range transport analyses over the open ocean, where no concentrated NO₂ emissions take place.

3 Methodology

To detect long-range transport events in a global dataset spanning five years of observation, we implemented an algorithm to find, verify and assess plumes from long-range transport events.

NO₂ long-range transport events in GOME-2 data

A. W. Zien et al.

Title Page

Abstract

Introduction

Conclusions

References

Tables

Figures



Back

Close

Full Screen / Esc

Printer-friendly Version

Interactive Discussion



3.1 Identification of potential long-range transport events

As a result of the short lifetime of NO₂ in the planetary boundary layer, observations from satellite show NO₂ to be strongly correlated to emission regions (Leue et al., 2001; Martin et al., 2002; Boersma et al., 2004; Richter et al., 2005; van der A et al., 2008). Long-time averages indicate emission and major outflow regions. NO₂ long-range transport events are isolated events that deviate from steady background pollution. During such an event plumes of NO₂ suddenly appear in the data and – if they persist long enough and observation conditions are favorable – move between subsequent observations.

Analysis of NO₂ long-range transport can be performed by just browsing through the data. For a more thorough and objective analysis, we need to enable computers to systematically find such events.

We therefore have developed an algorithm to identify intercontinental long-range transport events in maps of NO₂ vertical column densities. This algorithm builds on the following premises:

- long-range transport events are suddenly appearing and disappearing anomalies in the daily, global NO₂ observations,
- long-range transport events show extended NO₂ plumes which are composed of at least two pixels of 0.5° × 0.5°,
- long-range transport events can be traced back to source regions with lagrangian transport models.

To ensure that we recognize sudden features in the global timeseries, we compute a sliding mean and standard deviation for each day, which includes a number n_{days} of observations before and after the day in question. We do not include the day itself to avoid self-referencing of the plume.

For all further analysis, we only consider measurements over the oceans and mask out continental data. The oceans with their low NO_x sources allow us to see plumes

Title Page

Abstract

Introduction

Conclusions

References

Tables

Figures

◀

▶

◀

▶

Back

Close

Full Screen / Esc

Printer-friendly Version

Interactive Discussion



NO₂ long-range transport events in GOME-2 data

A. W. Zien et al.

Title Page

Abstract

Introduction

Conclusions

References

Tables

Figures

◀

▶

◀

▶

Back

Close

Full Screen / Esc

Printer-friendly Version

Interactive Discussion



clearly, whereas we might easily miss them over the continents or interpret varying emissions or effects of meteorological conditions on NO₂ observations as long-range transport events. Plumes over the ocean can only result from transport processes or stem from artifacts in the observations or retrieval. NO_x emissions from lightning are rarely detected in satellite data, due to both small vertical column densities and unfavorable viewing conditions (Beirle et al., 2009). Emissions from both ships and aircraft are too diluted and too frequent to appear as anomalous plumes in the data.

For each day, we select those pixels, which show NO₂ columns at least $n_{\text{seed}}\sigma$ above the mean. These are the candidate pixels. All candidate pixels within a great-circle distance $\Delta\theta$ of another pixel become seeds. All seeds within a distance of $\Delta\theta$ are merged. Pixels that have no neighbor within $\Delta\theta$ are discarded as outliers. The algorithm is illustrated in Fig. 4.

These seeds – containing two or more pixels – are now grown: all adjacent pixels which are at least $n_{\text{member}}\sigma$ above the mean are merged into the seed to form the plume. We iterate this process until no further pixels match the criteria. We discard all plumes that include less than $n_{\text{min,molec}}$ molecules of NO₂ for computational purposes and to filter out false positives from noise in the data.

For our analysis, we chose the following constants: $n_{\text{days}} = \pm 6$, $n_{\text{seed}} = 3$, $n_{\text{member}} = 2$, $\Delta\theta = 1.0^\circ$, and $n_{\text{min,molec}} = 5 \times 10^{30}$ molecules.

3.2 Backtracking of potential long-range transport events

Long-range transport events are dynamic processes. We perform backtracking of the plumes identified in the previous step. Then, we assess the properties of the plumes – in particular their altitude and origin – and discriminate between actual long-range transport events and artifacts from incomplete removal of stratospheric NO₂, the GOME-2 instrument or diurnal variation.

We employ the HYSPLIT_v4 lagrangian transport model (Draxler, 1999; Draxler and Hess, 1998, 2013) and supply it with Global Data Assimilation System (GDAS) (Na-

tional Climatic Data Center, NESDIS, NOAA, US Department of Commerce, 2006) meteorological data as input. For each plume, coordinates of all the associated pixels are inserted into HYSPLIT as starting points of back-trajectories. We do this at multiple altitude levels as we do not have any altitude information from the observations.

5 We select altitudes from 1000 m to 6000 m in steps of 500 m. HYSPLIT is then run backwards for 120 h – a little more than the reported NO₂ lifetime of up to four days in the free troposphere (Wenig et al., 2003) – and all the snapshots of the plumes (all associated points at 120 time steps and 11 altitude levels) are recorded.

10 For each of these snapshots we retrieve the seasonal mean tropospheric NO₂ vertical column density for each point that is within the planetary boundary layer (assumed to reach up to 1000 m). We obtain these values from the seasonally averaged cloud-free GOME-2 data from 2007 to 2011. A value of zero is recorded for points above the boundary layer. These values serve as a measure of the pollution which is available for transport at this point of the backtrajectory.

15 We compute a simple score for each snapshot to select the most likely source of the plume. This score implicitly favors a low dispersion of the points and thus also a young plume. It is computed as the number of trajectories that reside in the continental planetary boundary layer (below 1000 m a.s.l.) for every time step in the backtrajectory (snapshot).

20 We select the snapshot with the highest score to mark the beginning of the transport event and discard all snapshots from other altitudes and from all timesteps that go further back in time, leaving us only with the preferred trajectory.

3.3 Verification of potential long-range transport events

25 After we have determined the most likely trajectory, we assess whether or not this is actually a long-range transport event. We sum up the average seasonal clear-sky NO₂ vertical column density at the beginning of the trajectory of each pixel in the plume. The ratio between this measure of NO₂ pollution in the determined source region and

NO₂ long-range transport events in GOME-2 data

A. W. Zien et al.

Title Page

Abstract

Introduction

Conclusions

References

Tables

Figures



Back

Close

Full Screen / Esc

Printer-friendly Version

Interactive Discussion



the number of pixels in the plume has to exceed a minimum value in order to verify this plume as belonging to a long-range transport event.

We demand that the average source region pollution exceeds 5×10^{14} molecules cm^{-2} for a credible long-range transport event. This criterion is based on manual fine-tuning to find an optimum balance between obvious false positive and false negative events, by browsing through the results. All plumes that do not fulfill this criterion are discarded.

This method is feasible because we analyze plumes only over the ocean and assume that all source regions are located on the continents. While emissions from ships, airplanes and lightning contribute to the overall NO_2 budget, they are associated with significantly lower NO_2 vertical column densities than continental emissions, with an observed NO_2 vertical column density on the order of 10^{15} molecules cm^{-2} for the most polluted shipping lanes (Franke et al., 2009).

3.4 Assessment of properties

The aforementioned method allows us not only to identify transport-related NO_2 plumes but also to derive a number of properties for each individual long-range transport event. These properties include:

- the total area encompassed by the plume (from the extent of the pixels),
- the NO_2 content in each pixel (excess tropospheric NO_2 vertical column density above the sliding mean),
- the total NO_2 content in units of molecules or mass in GgN (by summing up vertical columns over the plume area),
- the source region of the plume,
- the age of the plume since it left the boundary layer,
- the altitude evolution of the plume from emission to observation,

NO_2 long-range transport events in GOME-2 data

A. W. Zien et al.

Title Page

Abstract

Introduction

Conclusions

References

Tables

Figures

◀

▶

◀

▶

Back

Close

Full Screen / Esc

Printer-friendly Version

Interactive Discussion



– the horizontal velocity of the plume.

In some cases, it is possible to identify the same plume at earlier or later time steps in the satellite data to get a more detailed analysis of such an event. Currently, we need to do this manually and therefore limit this part of the analysis to selected case studies.

4 Limitations

To apply the method outlined in the previous section, we have to limit the analysis to favorable conditions and assume simple long-range transport scenarios. There are a number of factors which contribute to the overall uncertainty of our developed method.

4.1 Satellite data

NO₂ observations from satellite are prone to retrieval errors, when trace gas absorption cross sections are fitted to the spectral radiance to retrieve the slant column density. With regard to the fit residual, we estimate the errors for an individual pixel to be on the order of 5×10^{14} molecules cm⁻² in equatorial regions, which amounts to up to a few percent. Plumes have to exceed an NO₂ content of 5×10^{30} molecules to be included in our study, which typically amounts to tens or hundreds of polluted pixels. This, together with the regridding of the data, partially mitigates the uncertainties.

The GOME-2 instruments measure only in daylight and cannot observe NO₂ during winter at high latitudes. This impedes the analysis of long-range transport events traveling to the Arctic, one of the most sensitive areas of interest for the long-range transport of air pollution (Sodemann et al., 2011).

4.2 Air-mass factors

To obtain NO₂ vertical column densities, we assume a profile that locates NO₂ between 3–5 km in altitude. Sensitivity studies show that the results for the NO₂ air-mass factor

NO₂ long-range transport events in GOME-2 data

A. W. Zien et al.

Title Page

Abstract

Introduction

Conclusions

References

Tables

Figures

◀

▶

◀

▶

Back

Close

Full Screen / Esc

Printer-friendly Version

Interactive Discussion



NO₂ long-range transport events in GOME-2 data

A. W. Zien et al.

Title Page

Abstract

Introduction

Conclusions

References

Tables

Figures

◀

▶

◀

▶

Back

Close

Full Screen / Esc

Printer-friendly Version

Interactive Discussion



do not vary strongly within this altitude range (Fig. 5). The standard deviation of air-mass factors for 2km thick layers of NO₂ mixed inside clouds for different altitudes is on the order of 3% for typical observation geometries. Variations of the thickness of the cloud and NO₂ layer have a similarly small effect.

Based on Crawford et al. (2003), we assume that the trace gas will be homogeneously mixed inside any cloud that may be present and stretch over an altitude range of 3–5 km during a long-range transport event. Our sensitivity studies show (Fig. 3) that the air-mass factor displays only small variance when a fraction of the trace gas is present above or below the cloud, as long as the majority is mixed inside the cloud. For this study, we chose the assumptions such that they produce the values near the center of the air-mass factors of all plausible NO₂-cloud-distributions.

Due to the lack of reliable information on the cloud profile, we use a homogeneous profile. We do not take the effects of aerosols explicitly into account, as long-range transport plumes tend to travel at elevated altitudes. This eliminates the effects of sea-spray. The effects of other aerosols should partially be mitigated by our cloud product. The remaining effect should be on the order of less than a few percent.

We do not take into account multi-layered clouds. In most cases, these would reduce the NO₂ signal and leave the plume or parts of it undetected by our algorithm. If NO₂ mixed inside a cloud would reside above another cloud, this could lead to an overestimation of NO₂ vertical column density due to an elongated light-path. This is not likely as most plumes tend to reside at relatively low altitudes.

4.3 Plume retrieval

The results of the long-range transport plume retrieval algorithm depend on its input parameters. The chosen thresholds and averaging windows are a result of manual inspection of satellite scenes and comparison to the results from the retrieval.

There are several parameters of interest:

- the σ -levels chosen for seed pixels and member pixels of a plume,

- the time frame for the sliding mean calculations,
- the maximum distance at which plumes are merged (i.e. the minimum distance of two distinct plumes).

Sensitivity studies show that the results are relatively stable with regards to these parameters. The used parameter sets were chosen to allow deriving a good result in reasonable computation time. Increasing the minimum distance between two distinct plumes will lead to slightly more plumes with high masses.

After plumes are retrieved, varying selection criteria for the preferred backtrajectory and varying verification criteria for the plume will lead to slightly different results. We have therefore implemented criteria that are as simple as possible while producing results that are consistent with manual inspection of a range of sample plumes.

The Lagrangian transport simulations we perform for each plume are also affected by uncertainties. Due to the coarse resolution of the used meteorological and NO₂ data – both vertically and horizontally – individual pixels will eventually diverge from the bulk in case of chaotic movement under conditions with strong winds. This is especially true for old plumes which provide the least reliable data. In most cases the bulk of the plume will stay relatively close together along the backtrajectory, so that stray pixels are not a problem.

We do not take plumes over the continents into account. There, fluctuating sources, albedo and topography make the analysis of continental long-range transport challenging. When we limit the analysis to the ocean, we have a data set that is much easier to interpret. However, we are prone to losing parts of plumes which are just on the shore. We also do not detect any continental plumes which do not move onto the ocean.

4.4 Lightning NO_x

There is another source of NO₂ over the ocean: lightning (Beirle et al., 2004). Schumann and Huntrieser (2007) report that approximately $5 \pm 3 \text{ Tg Na}^{-1}$ may originate from NO_x emitted by lightning (LiNO_x). Ott et al. (2010) show that NO_x concentrations in

NO₂ long-range transport events in GOME-2 data

A. W. Zien et al.

Title Page

Abstract

Introduction

Conclusions

References

Tables

Figures

◀

▶

◀

▶

Back

Close

Full Screen / Esc

Printer-friendly Version

Interactive Discussion



thunderstorm clouds may be higher than 10ppbv. They also show that only a small fraction of this LiNO_x is located in the cloud top, where the sensitivity of satellite observations is high. Instead, most of it is located in the lower parts of the cloud or below the cloud, where the sensitivity of satellite observations is low.

For this study we tried to locate major plumes of LiNO_x found in MOZAIC data (Savage et al., 2011). Only a very small fraction of these events was found in corresponding SCIAMACHY NO_2 satellite data, which was processed in the same way as the GOME-2 data in this study.

Additionally, the verification using backtrajecotires makes it unlikely that LiNO_x plumes are classified as long-range transport events in this study.

5 Case studies

To illustrate the nature of NO_2 long-range transport events and the successful application of the detection algorithm, we have selected four prominent samples from the collected set of events to scrutinize them in detail.

We use data from the NCEP/NCAR Reanalysis Project (Kalnay et al., 1996) to investigate meteorological conditions that accompany detected long-range transport events. Detailed properties of the plumes occurring during long-range transport events (for each observation) are given in Table 1.

5.1 North Atlantic, 17–19 December 2007

Figure 6 shows a striking example of an NO_2 long-range transport event in the western North Atlantic from 17 to 19 December 2007. Unfortunately, GOME-2 was operated in narrow-swath mode on 16 December 2007, so that we cannot observe how the plume separates from its emission region while being uplifted during the course of this day.

The NO_2 plume originates from the East Coast of North America, near the major emission regions of New York, Boston and Chicago. It closely follows the center

NO_2 long-range transport events in GOME-2 data

A. W. Zien et al.

Title Page

Abstract

Introduction

Conclusions

References

Tables

Figures

◀

▶

◀

▶

Back

Close

Full Screen / Esc

Printer-friendly Version

Interactive Discussion



NO₂ long-range transport events in GOME-2 data

A. W. Zien et al.

Title Page

Abstract

Introduction

Conclusions

References

Tables

Figures

◀

▶

◀

▶

Back

Close

Full Screen / Esc

Printer-friendly Version

Interactive Discussion



of a rapidly developing low-pressure system crossing the region from south-west to north-east. After two days, it crosses Newfoundland and subsequently disappears near Greenland in the Arctic night where GOME-2 cannot observe NO₂ vertical column densities. The origin and transport direction of this NO₂ long-range transport event are typical for this region and lie within the major storm track to the East of North America (Whittaker and Horn, 1984).

This mechanism of NO₂ long-range transport has been analyzed in a case study by Stohl et al. (2003). Unlike that study, here the NO₂ is centered on the cyclone as seen in NCEP DOE AMIP-II Reanalysis mean sea level pressure data. When we inspect further prominent long-range transport events emitted from the North American East Coast, we find that the NO₂ plumes typically follow a rapidly forming cyclone.

Such clear and long-lasting long-range transport events that can be observed for three consecutive days in GOME-2 data are rare. The reason for that lies in the combination of two phenomena:

- most long-range transport events form in the local winter when emission rates are high, low pressure systems are common, and NO₂ lifetime is long,
- long-range transport events tend to move polewards, if they do not dissolve.

This means that many long-lasting plumes will quickly move out of sight of the satellite instrument which cannot observe NO₂ in or near regions of polar night.

From our observations, we estimate the plume to contain roughly 2.31 GgN on the first day of observation. From the backtracing of the long-range transport event, we estimate the plume to be about 50 h old (since detaching from the planetary boundary layer) at the time of first observation. If we take photochemistry and dilution of the plume in the first 50 h into account, the amount of nitrogen exported from the continent in this event may have been significantly larger. Unfortunately, the few samples do not allow to estimate the lifetime of NO₂ in this event.

Further properties of the event are summarized in Table 1. We derive the minimum average travel speed of the plume (the actual speed will be higher due to curved trajec-

ories) from these properties, which amounted to 59 km h^{-1} from the first to the second observation. On the next day, we can only calculate a lower limit (32 km h^{-1}) due to the cut-off at polar night.

Figure 7 illustrates how closely the trajectory obtained from the backtracing algorithm matches the satellite observations of the plume at earlier times, even though all observations of an NO_2 plume are handled independently. Due to the coarse horizontal, vertical and temporal resolution of the meteorological data, the trajectory is not accurate on the outer rim of the plume; there, trajectories diverge from the main path.

5.2 South Africa, 9–12 July 2008

In the Southern Hemisphere, South Africa is the only region regularly emitting NO_2 long-range transport events. A clear event can be seen in the satellite data from 09 July 2008 emitted from the industrial region on the Highveld plateau. It follows the winds in the free troposphere towards the East for several days, disappearing after its last observation on 12 July 2008 near the Australian West Coast (Fig. 8).

South Africa has ideal conditions to create and observe long-range transport events. The Highveld plateau concentrates the nation's industry, injects factory and power plant exhausts at altitudes of more than 1500 m into the atmosphere, and is an isolated emission region. The prevailing north-westerly winds in this region propel elevated plumes onto the open ocean, which makes it easy to observe them with satellite measurements.

The selected long-range transport event is associated to a weak cyclone heading into the Antarctic. A cold front lifts the NO_2 plume up and their trajectories diverge subsequently. Winds of the free troposphere carry the plume straight to Australia.

We do not observe the plume entering Australia on 13 July 2008 due to a gap in the data and we do not find any traces of it on the following days. Upon arriving on shore the NO_2 may have descended and – due to shorter lifetime in the planetary boundary layer – dissipated. Also, rain may have washed out the NO_2 as HNO_3 .

NO_2 long-range transport events in GOME-2 data

A. W. Zien et al.

Title Page

Abstract

Introduction

Conclusions

References

Tables

Figures

◀

▶

◀

▶

Back

Close

Full Screen / Esc

Printer-friendly Version

Interactive Discussion



Due to the extent of this event, data gaps cover parts of the plume. This could explain why the measured NO_2 content of the plume increases from the first to the second day of observation.

>From the first to the second day of observation – while the plume follows the cyclone track – the average traveling speed is roughly 97 km h^{-1} . After the plume and the cyclone decouple, the plume only travels at 59 km h^{-1} and 51 km h^{-1} on consecutive days.

This plume bears similarities to the one analyzed by Wenig et al. (2003). The plume they observed crosses the ocean and arrives at Australia within five days which is consistent with the four consecutive observations in our data. They find thunderstorms with lightning coinciding with the plume on two observations, but the LiNO_x alone cannot explain the observed NO_2 vertical column densities in the plume. It might, however, replenish the plume and thereby increase its apparent lifetime.

Simulations with FLEXPART (Stohl et al., 2005), a more sophisticated lagrangian transport model, show the plume in their analysis to be traveling at altitudes from 2–6 km a.m.s.l. after it separated from the emission region in the Highveld plateau, which is consistent with our assumptions.

5.3 Australia, 27–30 April 2008

Australia only emits very few NO_2 plumes due to its limited emission sources, as compared with more populated and more heavily industrialized parts of the globe. However, we find a very long lasting long-range transport event in the data from 27–30 April 2008 which follows stationary wind patterns between a high-pressure system East of New Zealand and a low-pressure system over Antarctica. The plume disperses over the South Pacific ocean between two high-pressure systems (Fig. 9).

The size of this plume suggests that it could be caused by emissions from Australian bush fires. However, MODIS fire count data indicate that there were only few fires in South East and South West Australia. Most strong bush fires were located in North

NO_2 long-range transport events in GOME-2 data

A. W. Zien et al.

[Title Page](#)[Abstract](#)[Introduction](#)[Conclusions](#)[References](#)[Tables](#)[Figures](#)[◀](#)[▶](#)[◀](#)[▶](#)[Back](#)[Close](#)[Full Screen / Esc](#)[Printer-friendly Version](#)[Interactive Discussion](#)

Australia and it is questionable if the short lifetime of the NO_2 in these tropical latitudes would have allowed such a long transport.

Backtrajectories of the event indicate that the NO_2 may originate from the bush fires of both South East and South West Australia. NO_2 and glyoxal (CHOCHO) from large bush fires such as the Black Saturday fires are routinely observed in satellite data and GOME-2 data show elevated NO_2 vertical column densities over southwestern Australia on 25 and 26 April 2008 – on the order of 3×10^{15} molecules cm^{-2} , a factor two higher than background levels. It is likely, that our data product underestimates these values due to a lowered air-mass factor in the presence of black carbon aerosol in bush fire smoke plumes (Martin et al., 2003; Leitão et al., 2010; Giles et al., 2012). An origin in bush fires would also explain the necessary lifting of the NO_2 from the planetary boundary layer into the free troposphere in the absence of a frontal system (see Labonne et al., 2007).

The plume shows an exponential decay in NO_2 content – with a lifetime of approximately 28 h estimated from observations – even though parts of it are not visible in GOME-2 data. Extrapolating backwards to the time of emission, we estimate the NO_2 content to be about 10.5 GgN.

Data from the Lightning Imaging Sensor (LIS, Christian et al., 1999; Christian, 1999) show a small thunderstorm off the coast of Australia on both 27 and 28 April 2008, coinciding with the plume only on 27 April. It appears that the movement of the plume and the thunderstorm are not linked to each other. On 28 April and subsequent days, the plume travels outside the latitude range observed by LIS.

This long-range transport event also shows a deceleration over time. It starts with a minimum mean velocity of 105 km h^{-1} between the first two observations and decelerates to 74 km h^{-1} and 56 km h^{-1} on the consecutive days. This suggests that the NO_2 plume is stable even when the conditions leading to its emission diminish.

NO_2 long-range transport events in GOME-2 data

A. W. Zien et al.

Title Page

Abstract

Introduction

Conclusions

References

Tables

Figures

⏪

⏩

◀

▶

Back

Close

Full Screen / Esc

Printer-friendly Version

Interactive Discussion



5.4 Central Europe, 1–2 October 2010

Europe is a special case regarding long-range transport events. Due to local wind patterns, the NO₂ plumes are often ejected from the continent towards the north or north-west. Due to topography – strongly emitting regions located near the ocean in a bay – our algorithm retrieves very many long-range transport events here which are often very young at detection time.

On 1 and 2 October 2010 there is a prominent example of a long-range transport event in GOME-2 data. A small but elongated plume of NO₂ is emitted from the BeNeLux and Ruhr area when it is hit by a cyclone. The plume is transported onto the North Sea. It circles around the cyclone and is strongly filamented by the wind shear (see Fig. 10). On 3 October 2010 we can no longer identify the plume in the data. There is an apparent plume of NO₂ between Greenland and Svalbard, where observed NO₂ vertical column densities are highly variable. This anomaly is not detected in the algorithm as it shows no significant deviation above the sliding mean observations and cannot be directly related to a long-range transport event.

The observations suggest that the NO₂ in the plume is transported towards the center of the cyclone. Due to the strong shear winds in the cyclone, the plume is dispersed by 4 October 2010. It was not detected by our algorithm and is hardly discernable in visual inspection of the satellite data.

6 Statistical analysis

In the previous section, we described and analyzed well-defined examples of long-range transport events detected by our algorithm which were also found by visual inspection of the data. With the developed algorithm, however, we have the opportunity to analyze a larger dataset and use the automated detection of long-range transport events to perform statistical analyses of this phenomenon over a longer period.

NO₂ long-range transport events in GOME-2 data

A. W. Zien et al.

Title Page

Abstract

Introduction

Conclusions

References

Tables

Figures

◀

▶

◀

▶

Back

Close

Full Screen / Esc

Printer-friendly Version

Interactive Discussion



NO₂ long-range transport events in GOME-2 data

A. W. Zien et al.

Title Page

Abstract

Introduction

Conclusions

References

Tables

Figures

◀

▶

◀

▶

Back

Close

Full Screen / Esc

Printer-friendly Version

Interactive Discussion



The analysis found a total of 3808 verified NO₂ long-range transport events (out of a total of 8626 events) in the GOME-2 data from 2007 to 2011. Figure 11 shows their seasonal distribution for Northern and Southern Hemisphere. The distribution shows a strong seasonality in the frequency of long-range transport events; roughly half of all events occur during the local winter quarter. The Northern Hemisphere dominates the statistics due to more high-emission regions at higher latitudes.

We analyze the collection of long-range transport events from our algorithm to gain insight into favoring conditions, the hotspots and routes, and the range of parameters associated with them. First, we will focus on individual plumes' properties, then on ensemble properties.

6.1 Plume properties

Figure 12 shows that the NO₂ content of the plumes roughly follows an exponential distribution function:

$$d\rho(m) = \exp\left(-\frac{m}{m'}\right) dm, \quad (9)$$

where m is the NO₂ content of the plume and m' the scale mass of the distribution. A small scale mass indicates that small plumes dominate the distribution, while a large scale mass indicates that large plumes occur more regularly.

Looking only at the Northern Hemisphere (to exclude counteracting seasonality), we find that $m' = 0.25$ GgN for DJF, $m' = 0.24$ GgN for SON and $m' = 0.16$ GgN for MAM. Due to the low number of plumes, we could not determine m' for JJA.

Further analysis reveals that this distribution is relatively stable across the five years investigated. We did not detect any significant trend in the mass distributions.

The observed NO₂ content distribution is a result of the NO₂ content distribution at the time of emission and the age distribution coupled with the lifetime of NO₂ in such events. Plumes observed on multiple days will appear multiple times in this statistic.

The estimated age of the plumes (Fig. 13) follows a distribution that appears to be the result from three independent effects:

NO₂ long-range transport events in GOME-2 data

A. W. Zien et al.

Title Page

Abstract

Introduction

Conclusions

References

Tables

Figures

◀

▶

◀

▶

Back

Close

Full Screen / Esc

Printer-friendly Version

Interactive Discussion

– We find few plumes having ages of less than 24 h, as not many plumes will have fully separated from their emission region in this short time period. They are thus still residing in the area of the emission region's outflow, where high NO₂ vertical column density variability impedes their detection.

– After the age distribution reaches a maximum at about 18 h, the plume ages appear to be dominated by a decaying function which most likely results from dissociation, wash-out and dispersion of NO₂. This makes a detection by the algorithm less probable and incorporates a boundary between a plume and background NO₂.

– After about 96 h, the distribution increases again. This is probably a bias resulting from our detection algorithm. A higher plume age increases the chance of backtrajectories hitting an emission region. This may lead to an increase in false positive detections for high plume ages.

The distribution partly resembles a cumulative distribution function, as individual plumes may be observed on multiple, consecutive days (see Sect. 5). Plumes with an age approximately 24 h apart might actually be observations of the same plume on consecutive days. This effect is corrected for in the regional statistics (Sect. 6.3).

The altitude distribution (Fig. 14) behaves as expected: all plumes less than a day old reside at low altitudes, near their emission region. The plumes shift to higher altitudes on the second day. After that, the distribution broadens as long-range transport events take different paths. The distribution suggests, that – to minimize systematic errors – we might improve our NO₂ vertical column densities by employing a lower altitude range for the calculation of reflectivities and air-mass factors – both in presence and absence of clouds. However, as we have shown the impact of this deviation is small.

Investigations into the distribution of the area encompassed by long-range transport plumes shows that plumes of an age of two to three days at observation time cover the largest area (not shown). This indicates that plumes start with high NO₂ concentrations

and sharp boundaries, expand over a couple of days until the boundary of the plume gets blurred and the NO₂ content decreases.

6.2 Routes and sources

When browsing through the GOME-2 NO₂ data manually, long-range transport events tend to appear in particular regions and follow particular paths. With the derived dataset, we now verify this in a quantitative manner.

The first obvious analyses are the determination of the typical routes and their quantitative strength. To achieve this, we select the detected plumes from every day of observation and project their respective NO₂ content onto a global map. We sum up the NO₂ content from all plumes. This gives the total vertical column density of NO₂ in long-range transport events on a global map. Then, we divide by the total number of observations in the GOME-2 data set 2007–2011 for that particular grid cell (0.5° × 0.5°). This way, we obtain a global map of the 5 yr mean vertical column density of NO₂ in long-range transport events.

This will include plumes measured on multiple days and lead to an appropriate representation of the routes of longer-lasting plumes.

We perform this analysis for four seasons to illustrate the local seasonality of the phenomenon. The results can be seen in Fig. 15.

The data confirm the existence of hotspots of NO₂ long-range transport events in the mid-latitudes and typical transport routes along which NO₂ plumes travel. Note, that our algorithm only detects events over the ocean and routes over continental areas cannot be detected.

There is a strong seasonality in the data. Plumes are most dominant in local autumn and winter and can only rarely be seen in local summer. Due to observational limitations, especially the route of North American and European plumes towards the Arctic cannot be fully observed in the data. However, the data strongly suggest export of European and North American NO₂ to Greenland and onto the Arctic Ocean where it might alter tropospheric chemistry.

NO₂ long-range transport events in GOME-2 data

A. W. Zien et al.

Title Page

Abstract

Introduction

Conclusions

References

Tables

Figures

◀

▶

◀

▶

Back

Close

Full Screen / Esc

Printer-friendly Version

Interactive Discussion



NO₂ long-range transport events in GOME-2 data

A. W. Zien et al.

Title Page

Abstract

Introduction

Conclusions

References

Tables

Figures

◀

▶

◀

▶

Back

Close

Full Screen / Esc

Printer-friendly Version

Interactive Discussion



Long-range transport events are only observed in mid- to higher latitudes (starting roughly at $\pm 40^\circ$ N) where cyclones are frequent along the storm tracks and the lifetime of NO₂ is sufficiently long to allow transport over multiple days. We detect no significant long-range transport events in the tropics.

While China exports NO₂ quite frequently, not much of it is seen crossing a significant portion of the Pacific. Most of the plumes appear to be entering Russia after a brief journey over the ocean. This circular motion is typical for plumes in the Northern Hemisphere – North America and Europe show it to a lesser extent – and can be attributed to the cyclones transporting the plume.

We identify the sources of NO₂ long-range transport events by creating a similar map. Here, we project the NO₂ load of each pixel onto its origin, as determined by the last point in its backtrajectory. This produces a rough map of the relative source strength for NO₂ emitted into plumes of long-range transport events by that particular region. We show the map in Fig. 16.

We identify the following hot-spots: East Coast of North America, Central Europe, China, South Africa. Besides that, some plumes are also emitted from Argentina and Australia which only play a minor role. Europe is the only region that exhibits westward travel of plumes over the ocean.

The observations in South Africa indicate that some of the plumes might also originate in bush fires on the West Coast, while most stem from the Highveld plateau. A large fraction of backtrajectories end on the coast East of the plateau. This is most likely due to the elevated emissions and descending wind from the plateau down to the ocean.

Even though we use only verified long-range transports, the emission data are highly scattered. This is due to the chaotic deviations resulting from long backtrajectories in strong wind shear. The coarse resolution necessary for this study amplifies this effect. Keeping this in mind, it is surprising, how sharply the emitters of long-range transports observed over the ocean are localized.

Investigations into the sources for plumes at different observed ages show that sources for plumes in their first day are sharply defined and the determined sources become more scattered with each day of plume age.

Figure 17 shows an analogous map to Fig. 15, but here the NO₂ vertical column densities in long-range transport plumes are averaged over all seasons and instead binned by their respective plume age to show the temporal evolution of the routes. As expected, we find plumes with older ages at observation time at a larger distance from the emission regions and spread out more broadly than the young plumes. Also, the large number of plumes in the Baltic and North Sea, enclosed by emission regions (see Sect. 5.4), is apparent.

6.3 Regions

There are four major regions emitting NO₂ long-range transport events on the globe: the North American East Coast, Central Europe, South Africa and China. We have analyzed the plumes from these regions in further detail to gain more insight into the atmospheric conditions during long-range transport events and to quantify their impact on the global NO₂ distribution. The regions are highlighted in Fig. 18.

For each region, we only select plumes that moved from a continental area in the emission region out to the ocean in the observation region within the last 24 h. This way, we make sure that no plumes are counted twice and we only select plumes that actually originate in the selected hot-spot region.

The frequency of long-range transport events differs strongly from region to region. North America and Europe emit a plume every 10 days on annual average, which corresponds to one plume every 5 days during winter. In contrast to that, South Africa emits plumes only every 17 days, while China emits one plume a week. This illustrates that NO₂ long-range transport is not a rare phenomenon and has been hidden from systematic scientific scrutiny only by cloud-filtering of satellite data.

NO₂ long-range transport events in GOME-2 data

A. W. Zien et al.

Title Page

Abstract

Introduction

Conclusions

References

Tables

Figures

◀

▶

◀

▶

Back

Close

Full Screen / Esc

Printer-friendly Version

Interactive Discussion



6.3.1 Boundary NO₂ flux

First, we analyze the boundary flux of these regions. We sum up the NO₂ content of all the plumes in the respective region and normalize by the number of days of observation. This yields the total yearly export of NO₂ from the continent onto the ocean.

The data in Fig. 19 show, that the strongest emitter of plumes is China, followed by Europe. However, the plumes from China do not last as long and do not form such a prominent route. It appears that South Africa experiences the opposing effect: here, plumes follow a very stable and visible route over the open ocean. This leads to small absolute emissions being strongly represented in the dataset.

The total outflux of these four regions amounts to more than 50GgNa⁻¹ in long-range transport events, which are exported to the ocean and remote regions. This is slightly more than a permil of the estimated global yearly NO₂ emission rate of 43TgNa⁻¹. This might appear to be a small fraction, but it constitutes a significant amount for such an unstable gas – especially, as our backtracing algorithm does not take the decay of NO₂ from emission to observation of the plume into account.

We also look at the regional differences in plume sizes. Figure 20 shows that China and especially Europe emit a relatively large fraction of NO₂-rich long-range transport plumes. North America and South Africa tend to produce much smaller plumes.

6.3.2 Composite analysis of meteorological conditions

Finally, we take a look into large-scale meteorological conditions which accompany long-range transport events, using NCEP DOE AMIP-II Reanalysis data. We use a composite analysis which has been used in similar studies to analyze polar lows in the nordic seas (Blechschmidt et al., 2009) and NO_x transport in South Africa (Abiodun et al., 2013).

For each long-range transport event that we find in the given region, we collect meteorological conditions for various temporal offsets: two days before the plume has been

NO₂ long-range transport events in GOME-2 data

A. W. Zien et al.

Title Page

Abstract

Introduction

Conclusions

References

Tables

Figures

⏪

⏩

◀

▶

Back

Close

Full Screen / Esc

Printer-friendly Version

Interactive Discussion



**NO₂ long-range
transport events in
GOME-2 data**

A. W. Zien et al.

Title Page

Abstract

Introduction

Conclusions

References

Tables

Figures

◀

▶

◀

▶

Back

Close

Full Screen / Esc

Printer-friendly Version

Interactive Discussion



emitted (according to backtrajectories) until the date of observation. For each offset we iterate over all retrieved long-range transport events and collect the meteorological conditions at the respective offset from emission (we call this the related composite). All remaining observations are collected in the unrelated composite. This allows an analysis of the temporal evolution of the conditions and yields insight into the dominant meteorological conditions behind long-range transport events.

We allow for multiple observations of the same plume to enter the dataset as these stronger and more reliable events are a better indication of favorable conditions.

We restrict the analysis to the respective winter seasons: December, January and February (DJF) in the Northern Hemisphere; June, July and August (JJA) in the Southern Hemisphere. These are the months with the highest long-range transport event frequency and thus most suited to investigate the associated meteorological conditions.

Now, for various meteorological quantities, we have two disjoint sets of observations (or composites): observations related and unrelated to plume emission. The unrelated composite represents the climatological mean in the absence of NO₂ long-range transport events. We calculate the deviation of the average of both the related and the unrelated composite. Also, we use the Mann–Whitney U test (Mann and Whitney, 1947) to find significant deviations in the two distributions.

We perform this test for the mean sea level pressure, the surface air temperature, the FRESCO+ cloud fraction and the NO₂ vertical column density. Note that for the composite analysis, we did not interpolate values from NCEP DOE AMIP-II Reanalysis and GOME-2 and instead selected the nearest time step in the respective data set. This may lead to temporal discrepancies of up to 12 h between the two data sets as we evaluate GOME-2 data only once a day.

North America (not shown) shows only very weak anomalies in these data – showing a slightly higher pressure over the central Atlantic – which do not provide further insight into the development of long-range transport events.

NO₂ long-range transport events in GOME-2 data

A. W. Zien et al.

Title Page

Abstract

Introduction

Conclusions

References

Tables

Figures

◀

▶

◀

▶

Back

Close

Full Screen / Esc

Printer-friendly Version

Interactive Discussion



In South Africa, we find that in the days preceding the emission of the plume, there is a significant (likelihood > 99%) alternating pattern of sea-level pressure anomalies (Fig. 21) in the region of 30–60° S, surrounding the Antarctic continent. These anomalies are of the order $|\Delta P| \approx 2\text{--}5$ hPa and move eastwards during the lifetime of long-range transport events, indicating low-pressure systems passing South Africa.

Composites of GOME-2 observations show elevated NO₂ vertical column densities over the Highveld plateau, moving to the south-east over the lifetime of a long-range transport event (Fig. 22). After the plume is emitted, NO₂ vertical column densities show an anomaly towards lower values in the Highveld region.

In Europe (Fig. 23), the situation is similar. In the days preceding a long-range transport event there is significantly reduced mean sea-level pressure over Western Europe of the order $\Delta P \approx -4 \dots -8$ hPa. There is a significant low surface temperature anomaly over Europe and northern Russia in the preceding days, of order $\Delta T \approx -2 \dots -5$ K. Additionally, in the composite, we observe regions of higher pressure over Scandinavia, which extend up to the Arctic on subsequent days. These patterns are stationary and indicate high wind speeds towards the north-west in the transition region between the high- and low-pressure pattern. This represents the dominant route of European long-range transport plumes, we find in this study.

Eckhardt et al. (2003) have shown in simulations that the North Atlantic Oscillation (NAO) may be responsible for transport of pollutants to the Arctic, modeling trace gases with lifetimes of 5 days. Christoudias et al. (2012) find similar patterns of pollution export as shown in Fig. 15 to stem from zonal wind flow, resulting from the NAO. However, a correlation of plume frequency with monthly NAO indices from the NCEP Climate Prediction Center (<http://www.cpc.ncep.noaa.gov/products/precip/CWlink/>) shows no significant correlation and Fig. 23 shows no NAO characteristics.

For long-range transport events originating from Europe, we find significantly elevated NO₂ vertical column densities over Europe, the North Sea and the North East Atlantic during the course of emission.

the boundary layer, where most emissions take place. Unfortunately, GOME-2 satellite data do not permit an analysis of these processes in the Arctic.

The emission shows strong seasonality, both in number and size of the plumes. More and larger plumes are emitted in winter, when the lifetime of NO_2 is long, anthropogenic emission rates are especially high and meteorological conditions are favorable with frequent cold fronts and cyclones. No long-range transport events have been identified in the tropics.

The meteorology responsible for these events appears to depend on the region. In North America, plumes follow storm tracks over the Atlantic, but show no distinct meteorological anomaly in a composite analysis. In Europe, Arctic highs and European lows appear to favor long-range transports towards the Arctic. South Africa shows a typical pattern of alternating high and low pressure systems moving eastwards linked to plume emission.

It is likely that many events are triggered by a cyclone passing the emission region, accompanied by a cold front which lifts the NO_2 upwards into the free troposphere. There, wind speeds tend to be higher and the lifetime of NO_2 increases to the order of days, which is consistent with what we find in observations. Plumes can keep their distinct boundaries over days before they dilute.

Besides events from anthropogenic sources, we also observe events from Australia which appear to be caused by bushfires in the south of the continent.

NO_2 long-range transport events can transport air pollution from South Africa to Australia, from China to Japan and Taiwan and they are likely to have an impact on remote, pristine regions such as the Arctic.

Acknowledgements. This work is part of the INTAS project. It was inspired by work of Andreas Heckel, see http://www.doas-bremen.de/posters/egu_2005_heckel.pdf. We gratefully acknowledge the funding by the Deutsche Forschungsgemeinschaft (DFG) and Universität Bremen. GOME-2 radiances have been provided by EUMETSAT. NCEP Reanalysis data provided by the NOAA/OAR/ESRL PSD, Boulder, Colorado, USA, from their web site at <http://www.esrl.noaa.gov/psd/>. NCEP EDAS and GDAS (FNL) Model Data (DSI-6141) provided by the NOAA/NCDC, Asheville, NC, USA, from their web site at <http://www.ncdc.noaa.gov>. The

NO₂ long-range transport events in GOME-2 data

A. W. Zien et al.

Title Page

Abstract

Introduction

Conclusions

References

Tables

Figures



Back

Close

Full Screen / Esc

Printer-friendly Version

Interactive Discussion



HYSPLIT model was provided by the NOAA/ARL. We gratefully acknowledge Stefan Schreier's advice on biomass burning in Australia.

References

- Abiodun, B. J., Ojumu, A. M., Jenner, S., and Ojumu, T. V.: Transport of atmospheric NO_x and HNO₃ over Cape Town, *Atmos. Chem. Phys. Discuss.*, 13, 11827–11862, doi:10.5194/acpd-13-11827-2013, 2013. 30977
- Aschmann, J., Sinnhuber, B.-M., Atlas, E. L., and Schaufli, S. M.: Modeling the transport of very short-lived substances into the tropical upper troposphere and lower stratosphere, *Atmos. Chem. Phys.*, 9, 9237–9247, doi:10.5194/acp-9-9237-2009, 2009. 30953
- Beirle, S., Platt, U., Wenig, M., and Wagner, T.: NO_x production by lightning estimated with GOME, *Adv. Space Res.*, 34, 793–797, doi:10.1016/j.asr.2003.07.069, 2004. 30965
- Beirle, S., Salzmann, M., Lawrence, M. G., and Wagner, T.: Sensitivity of satellite observations for freshly produced lightning NO_x, *Atmos. Chem. Phys.*, 9, 1077–1094, doi:10.5194/acp-9-1077-2009, 2009. 30960
- Beirle, S., Boersma, K. F., Platt, U., Lawrence, M. G., and Wagner, T.: Megacity emissions and lifetimes of nitrogen oxides probed from space, *Science*, 333, 1737–1739, doi:10.1126/science.1207824, 2011. 30947
- Blechschmidt, A.-M., Bakan, S., and Graßl, H.: Large-scale atmospheric circulation patterns during polar low events over the Nordic seas, *J. Geophys. Res.-Atmos.*, 114, D06115, doi:10.1029/2008JD010865, 2009. 30977
- Boersma, K. F., Eskes, H. J., and Brinksma, E. J.: Error analysis for tropospheric NO₂ retrieval from space, *J. Geophys. Res.-Atmos.*, 109, D04311, doi:10.1029/2003JD003962, 2004. 30959
- Bovensmann, H., Burrows, J. P., Buchwitz, M., Frerick, J., Noël, S., Rozanov, V. V., Chance, K. V., and Goede, A. P. H.: SCIAMACHY: mission objectives and measurement modes, *J. Atmos. Sci.*, 56, 127–150, doi:10.1175/1520-0469(1999)056<0127:SMOAMM>2.0.CO;2, 1999. 30951
- Burrows, J., Hölzle, E., Goede, A., Visser, H., and Fricke, W.: SCIAMACHY – scanning imaging absorption spectrometer for atmospheric cartography, *Acta Astronaut.*, 35, 445–451, doi:10.1016/0094-5765(94)00278-T, 1995. 30951

NO₂ long-range transport events in GOME-2 data

A. W. Zien et al.

Title Page

Abstract

Introduction

Conclusions

References

Tables

Figures

◀

▶

◀

▶

Back

Close

Full Screen / Esc

Printer-friendly Version

Interactive Discussion



NO₂ long-range transport events in GOME-2 data

A. W. Zien et al.

Title Page

Abstract

Introduction

Conclusions

References

Tables

Figures

◀

▶

◀

▶

Back

Close

Full Screen / Esc

Printer-friendly Version

Interactive Discussion



Burrows, J. P., Weber, M., Buchwitz, M., Rozanov, V., Ladstätter-Weißenmayer, A., Richter, A., DeBeek, R., Hoogen, R., Bramstedt, K., Eichmann, K.-U., Eisinger, M., and Perner, D.: The Global Ozone Monitoring Experiment (GOME): mission concept and first scientific results, *J. Atmos. Sci.*, 56, 151–175, doi:10.1175/1520-0469(1999)056<0151:TGOMEG>2.0.CO;2, 1999. 30951

Callies, J., Corpaccioli, E., Eisinger, M., Hahne, A., and Lefebvre, A.: GOME-2 – Metop’s Second Generation sensor for Operational Ozone Monitoring, *ESA Bulletin*, 102, 2000. 30951

Christian, H. J.: Optical detection of lightning from space, in: Proceedings of the 11th International Conference on Atmospheric Electricity, Guntersville, Alabama, 715–718, available at: <http://thunder.nsstc.nasa.gov/lis/> (last access: 12 September 2013), 7–11 June 1999. 30970

Christian, H. J., Blakeslee, R. J., Goodman, S. J., Mach, D. A., Stewart, M. F., Buechler, D. E., Koshak, W. J., Hall, J. M., Boeck, W. L., Driscoll, K. T., and Bocippio, D. J.: The Lightning Imaging Sensor, in: Proceedings of the 11th International Conference on Atmospheric Electricity, Guntersville, Alabama, 746–749, available at: http://thunder.nsstc.nasa.gov/bookshelf/pubs/LIS_ICAE99_Print.pdf (last access: 12 September 2013), 7–11 June 1999. 30970

Christoudias, T., Pozzer, A., and Lelieveld, J.: Influence of the North Atlantic Oscillation on air pollution transport, *Atmos. Chem. Phys.*, 12, 869–877, doi:10.5194/acp-12-869-2012, 2012. 30979

Crawford, J., Olson, J., Davis, D., Chen, G., Barrick, J., Shetter, R., Lefer, B., Jordan, C., Anderson, B., Clarke, A., Sachse, G., Blake, D., Singh, H., Sandolm, S., Tan, D., Kondo, Y., Avery, M., Flocke, F., Eisele, F., Mauldin, L., Zondlo, M., Brune, W., Harder, H., Martinez, M., Talbot, R., Bandy, A., and Thornton, D.: Clouds and trace gas distributions during TRACE-P, *J. Geophys. Res.*, 108, 8818, doi:10.1029/2002JD003177, 2003. 30957, 30964

Dentener, F., Keating, T., and Akimoto, H.: Hemispheric transport of air pollution, Tech. rep., United Nations, Geneva, available at: http://htap.org/publications/2010_report/2010_Final_Report/HTAP2010PartA110407.pdf (last access: 14 August 2013), 2010. 30949

Draxler, R.: HYSPLIT4 User’s Guide, NOAA Tech. Memo. ERL ARL-230, NOAA Air Resources Laboratory, Silver Spring, MD, 1999. 30960

Draxler, R. and Hess, G.: Description of the HYSPLIT_4 modeling system, NOAA Tech. Memo. ERL ARL-224, NOAA Air Resources Laboratory, Silver Spring, MD, 1997. 30960

Draxler, R. and Hess, G.: An overview of the HYSPLIT_4 modeling system of trajectories, dispersion, and deposition, *Aust. Meteor. Mag.*, 47, 295–308, 1998. 30960

NO₂ long-range transport events in GOME-2 data

A. W. Zien et al.

Title Page

Abstract

Introduction

Conclusions

References

Tables

Figures

◀

▶

◀

▶

Back

Close

Full Screen / Esc

Printer-friendly Version

Interactive Discussion



- Eckhardt, S., Stohl, A., Beirle, S., Spichtinger, N., James, P., Forster, C., Junker, C., Wagner, T., Platt, U., and Jennings, S. G.: The North Atlantic Oscillation controls air pollution transport to the Arctic, *Atmos. Chem. Phys.*, 3, 1769–1778, doi:10.5194/acp-3-1769-2003, 2003. 30979
- 5 Ehhalt, D. H., Rohrer, F., and Wahner, A.: Sources and distribution of NO_x in the upper troposphere at northern mid-latitudes, *J. Geophys. Res.*, 97, 3725–3738, 1992. 30947
- Eskes, H. J. and Boersma, K. F.: Averaging kernels for DOAS total-column satellite retrievals, *Atmos. Chem. Phys.*, 3, 1285–1291, doi:10.5194/acp-3-1285-2003, 2003. 30955
- 10 Franke, K., Richter, A., Bovensmann, H., Eyring, V., Jöckel, P., Hoor, P., and Burrows, J. P.: Ship emitted NO₂ in the Indian Ocean: comparison of model results with satellite data, *Atmos. Chem. Phys.*, 9, 7289–7301, doi:10.5194/acp-9-7289-2009, 2009. 30962
- Giles, D. M., Holben, B. N., Eck, T. F., Sinyuk, A., Smirnov, A., Slutsker, I., Dickerson, R. R., Thompson, A. M., and Schafer, J. S.: An analysis of AERONET aerosol absorption properties and classifications representative of aerosol source regions, *J. Geophys. Res.-Atmos.*, 117, D17203, doi:10.1029/2012JD018127, 2012. 30970
- 15 Hilboll, A., Richter, A., and Burrows, J. P.: Long-term changes of tropospheric NO₂ over megacities derived from multiple satellite instruments, *Atmos. Chem. Phys.*, 13, 4145–4169, doi:10.5194/acp-13-4145-2013, 2013. 30953
- Hild, L., Richter, A., Rozanov, V., and Burrows, J. P.: Air mass factor calculations for GOME measurements of lightning-produced NO₂, *Adv. Space Res.*, 29, 1685–1690, doi:10.1016/S0273-1177(02)80014-X, 2002. 30955
- 20 Horowitz, L. W., Walters, S., Mauzerall, D. L., Emmons, L. K., Rasch, P. J., Granier, C., Tie, X., Lamarque, J.-F., Schultz, M. G., Tyndall, G. S., Orlando, J. J., and Brasseur, G. P.: A global simulation of tropospheric ozone and related tracers: description and evaluation of MOZART, version 2, *J. Geophys. Res.-Atmos.*, 108, 4784, doi:10.1029/2002JD002853, 2003. 30957
- 25 Kalnay, E., Kanamitsu, M., Kistler, R., Collins, W., Deaven, D., Gandin, L., Iredell, M., Saha, S., White, G., Woollen, J., Zhu, Y., Leetmaa, A., Reynolds, R., Chelliah, M., Ebisuzaki, W., Higgins, W., Janowiak, J., Mo, K. C., Ropelewski, C., Wang, J., Jenne, R., and Joseph, D.: The NCEP/NCAR 40-year reanalysis project, *B. Am. Meteorol. Soc.*, 77, 437–470, 1996. 30966
- 30 Kokhanovsky, A. and Rozanov, V.: Retrieval of NO₂ vertical columns under cloudy conditions: a sensitivity study based on SCIATRAN calculations, *Atmos. Res.*, 93, 695–699, doi:10.1016/j.atmosres.2009.01.022, 2009. 30957

NO₂ long-range transport events in GOME-2 data

A. W. Zien et al.

Title Page

Abstract

Introduction

Conclusions

References

Tables

Figures

◀

▶

◀

▶

Back

Close

Full Screen / Esc

Printer-friendly Version

Interactive Discussion



Labonne, M., Bréon, F.-M., and Chevallier, F.: Injection height of biomass burning aerosols as seen from a spaceborne lidar, *Geophys. Res. Lett.*, 34, doi:10.1029/2007GL029311, 2007. 30970

Leitão, J., Richter, A., Vrekoussis, M., Kokhanovsky, A., Zhang, Q. J., Beekmann, M., and Burrows, J. P.: On the improvement of NO₂ satellite retrievals – aerosol impact on the air mass factors, *Atmos. Meas. Tech.*, 3, 475–493, doi:10.5194/amt-3-475-2010, 2010. 30970

Leue, C., Wenig, M., Wagner, T., Klimm, O., Platt, U., and Jähne, B.: Quantitative analysis of NO_x emissions from Global Ozone Monitoring Experiment satellite image sequences, *J. Geophys. Res.-Atmos.*, 106, 5493–5505, doi:10.1029/2000JD900572, 2001. 30959

Lin, M., Holloway, T., Carmichael, G. R., and Fiore, A. M.: Quantifying pollution inflow and outflow over East Asia in spring with regional and global models, *Atmos. Chem. Phys.*, 10, 4221–4239, doi:10.5194/acp-10-4221-2010, 2010. 30950

Mann, H. B. and Whitney, D. R.: On a test of whether one of two random variables is stochastically larger than the other, *Ann. Math. Stat.*, 18, 50–60, doi:10.1214/aoms/1177730491, 1947. 30978

Martin, R. V., Chance, K., Jacob, D. J., Kurosu, T. P., Spurr, R. J. D., Bucsela, E., Gleason, J. F., Palmer, P. I., Bey, I., Fiore, A. M., Li, Q., Yantosca, R. M., and Koelemeijer, R. B. A.: An improved retrieval of tropospheric nitrogen dioxide from GOME, *J. Geophys. Res.-Atmos.*, 107, 4437, doi:10.1029/2001jd001027, 2002. 30959

Martin, R. V., Jacob, D. J., Chance, K., Kurosu, T. P., Palmer, P. I., and Evans, M. J.: Global inventory of nitrogen oxide emissions constrained by space-based observations of NO₂ columns, *J. Geophys. Res.-Atmos.*, 108, 4537, doi:10.1029/2003JD003453, 2003. 30947, 30970

National Climatic Data Center, NESDIS, NOAA, US Department of Commerce: NCEP EDAS and GDAS (FNL) Model Data (DSI-6141), available at: <http://www.ncdc.noaa.gov> (last access: 18 February 2013), 2006. 30960

Ott, L. E., Pickering, K. E., Stenchikov, G. L., Allen, D. J., DeCaria, A. J., Ridley, B., Lin, R.-F., Lang, S., and Tao, W.-K.: Production of lightning NO_x and its vertical distribution calculated from three-dimensional cloud-scale chemical transport model simulations, *J. Geophys. Res.-Atmos.*, 115, D04301, doi:10.1029/2009JD011880, 2010. 30965

Palmer, P. I., Jacob, D. J., Chance, K., Martin, R. V., Spurr, R. J. D., Kurosu, T. P., Bey, I., Yantosca, R., Fiore, A., and Li, Q.: Air mass factor formulation for spectroscopic measurements from satellites: application to formaldehyde retrievals from the Global Ozone Monitoring Ex-

NO₂ long-range transport events in GOME-2 data

A. W. Zien et al.

Title Page

Abstract

Introduction

Conclusions

References

Tables

Figures

◀

▶

◀

▶

Back

Close

Full Screen / Esc

Printer-friendly Version

Interactive Discussion



periment, *J. Geophys. Res.-Atmos.*, 106, 14539–14550, doi:10.1029/2000JD900772, 2001. 30954

Platt, U. and Stutz, J.: *Differential Optical Absorption Spectroscopy: Principles and Applications*, 1st edn., Springer, Berlin, 2007. 30951

5 Popp, C., Wang, P., Brunner, D., Stammes, P., Zhou, Y., and Grzegorski, M.: MERIS albedo climatology for FRESCO+ O₂ A-band cloud retrieval, *Atmos. Meas. Tech.*, 4, 463–483, doi:10.5194/amt-4-463-2011, 2011. 30956

Rastigejev, Y., Park, R., Brenner, M. P., and Jacob, D. J.: Resolving intercontinental pollution plumes in global models of atmospheric transport, available at: <http://www.agu.org/pubs/crossref/2010/2009JD012568.shtml> (last access: 27 January 2010), 2010. 30948, 30957

10 Richter, A. and Burrows, J. P.: Tropospheric NO₂ from GOME measurements, *Adv. Space Res.*, 29, 1673–1683, doi:10.1016/S0273-1177(02)00100-X, 2002. 30952, 30953

Richter, A., Burrows, J. P., Nüß, H., Granier, C., and Niemeier, U.: Increase in tropospheric nitrogen dioxide over China observed from space, *Nature*, 437, 129–132, doi:10.1038/nature04092, 2005. 30959

15 Richter, A., Begoin, M., Hilboll, A., and Burrows, J. P.: An improved NO₂ retrieval for the GOME-2 satellite instrument, *Atmos. Meas. Tech.*, 4, 1147–1159, doi:10.5194/amt-4-1147-2011, 2011. 30952

Riuttanen, L., Dal Maso, M., de Leeuw, G., Riipinen, I., Sogacheva, L., Vakkari, V., Laakso, L., and Kulmala, M.: Long-range transport of biomass burning smoke to Finland in 2006, *Atmos. Chem. Phys. Discuss.*, 13, 4289–4330, doi:10.5194/acpd-13-4289-2013, 2013. 30950

20 Rozanov, A., Rozanov, V., Buchwitz, M., Kokhanovsky, A., and Burrows, J.: SCIATRAN 2.0 – a new radiative transfer model for geophysical applications in the 175–2400 nm spectral region, *Adv. Space Res.*, 36, 1015–1019, doi:10.1016/j.asr.2005.03.012, 2005. 30954

25 Rozanov, V., Rozanov, A., Kokhanovsky, A., and Burrows, J.: Radiative transfer through terrestrial atmosphere and ocean: software package SCIATRAN, *J. Quant. Spectrosc. Ra.*, 133, 13–71, doi:10.1016/j.jqsrt.2013.07.004, 2013. 30954

Sauvage, B., Cammas, J., Defer, E., Volz-Thomas, A., Thomas, K., and Holle, R. L.: Lightning NO_x influence on large scale NO_y and O₃ plumes observed over the northern mid-latitudes, *AGU Fall Meeting Abstracts*, -1, 0187, available at: <http://adsabs.harvard.edu/abs/2011AGUFM.A51A0187S> (last access: 14 August 2013), 2011. 30966

30 Schaub, D., Weiss, A. K., Kaiser, J. W., Petritoli, A., Richter, A., Buchmann, B., and Burrows, J. P.: A transboundary transport episode of nitrogen dioxide as observed from GOME

**NO₂ long-range
transport events in
GOME-2 data**

A. W. Zien et al.

Title Page

Abstract

Introduction

Conclusions

References

Tables

Figures

◀

▶

◀

▶

Back

Close

Full Screen / Esc

Printer-friendly Version

Interactive Discussion



and its impact in the Alpine region, *Atmos. Chem. Phys.*, 5, 23–37, doi:10.5194/acp-5-23-2005, 2005. 30950

Schultz, M., Schmitt, R., Thomas, K., and Volz-Thomas, A.: Photochemical box modeling of long-range transport from North America to Tenerife during the North Atlantic Regional Experiment (NARE) 1993, *J. Geophys. Res.*, 103, 13477–13488, doi:10.1029/97JD01481, 1998. 30948

Schumann, U. and Huntrieser, H.: The global lightning-induced nitrogen oxides source, *Atmos. Chem. Phys.*, 7, 3823–3907, doi:10.5194/acp-7-3823-2007, 2007. 30965

Singh, H. B. and Hanst, P. L.: Peroxyacetyl nitrate (PAN) in the unpolluted atmosphere: An important reservoir for nitrogen oxides, *Geophys. Res. Lett.*, 8, 941–944, doi:10.1029/GL008i008p00941, 1981. 30948

Sodemann, H., Pommier, M., Arnold, S. R., Monks, S. A., Stebel, K., Burkhardt, J. F., Hair, J. W., Diskin, G. S., Clerbaux, C., Coheur, P.-F., Hurtmans, D., Schlager, H., Blechschmidt, A.-M., Kristjánsson, J. E., and Stohl, A.: Episodes of cross-polar transport in the Arctic troposphere during July 2008 as seen from models, satellite, and aircraft observations, *Atmos. Chem. Phys.*, 11, 3631–3651, doi:10.5194/acp-11-3631-2011, 2011. 30963

Solomon, S., Schmeltekopf, A. L., and Sanders, R. W.: On the interpretation of zenith sky absorption measurements, *J. Geophys. Res.*, 92, 8311–8319, 1987. 30951

Spichtinger, N., Wenig, M., James, P., Wagner, T., Platt, U., and Stohl, A.: Satellite detection of a continental-scale plume of nitrogen oxides from boreal forest fires, *Geophys. Res. Lett.*, 28, 4579–4582, 2001. 30950

Stohl, A., Huntrieser, H., Richter, A., Beirle, S., Cooper, O. R., Eckhardt, S., Forster, C., James, P., Spichtinger, N., Wenig, M., Wagner, T., Burrows, J. P., and Platt, U.: Rapid intercontinental air pollution transport associated with a meteorological bomb, *Atmos. Chem. Phys.*, 3, 969–985, doi:10.5194/acp-3-969-2003, 2003. 30949, 30967

Stohl, A., Forster, C., Frank, A., Seibert, P., and Wotawa, G.: Technical note: The Lagrangian particle dispersion model FLEXPART version 6.2, *Atmos. Chem. Phys.*, 5, 2461–2474, doi:10.5194/acp-5-2461-2005, 2005. 30969

van der A, R. J., Eskes, H. J., Boersma, K. F., van Noije, T. P. C., Van Roozendael, M., De Smedt, I., Peters, D. H. M. U., and Meijer, E. W.: Trends, seasonal variability and dominant NO_x source derived from a ten year record of NO₂ measured from space, *J. Geophys. Res.-Atmos.*, 113, D04302, doi:10.1029/2007JD009021, 2008. 30959

**NO₂ long-range
transport events in
GOME-2 data**

A. W. Zien et al.

[Title Page](#)[Abstract](#)[Introduction](#)[Conclusions](#)[References](#)[Tables](#)[Figures](#)[⏪](#)[⏩](#)[◀](#)[▶](#)[Back](#)[Close](#)[Full Screen / Esc](#)[Printer-friendly Version](#)[Interactive Discussion](#)

Walker, T. W., Martin, R. V., van Donkelaar, A., Leaitch, W. R., MacDonald, A. M., Anlauf, K. G.,
Cohen, R. C., Bertram, T. H., Huey, L. G., Avery, M. A., Weinheimer, A. J., Flocke, F. M.,
Tarasick, D. W., Thompson, A. M., Streets, D. G., and Liu, X.: Trans-Pacific transport of
reactive nitrogen and ozone to Canada during spring, *Atmos. Chem. Phys.*, 10, 8353–8372,
doi:10.5194/acp-10-8353-2010, 2010. 30948

Wang, P., Stammes, P., van der A, R., Pinardi, G., and van Roozendael, M.: FRESCO+: an
improved O₂ A-band cloud retrieval algorithm for tropospheric trace gas retrievals, *Atmos.*
Chem. Phys., 8, 6565–6576, doi:10.5194/acp-8-6565-2008, 2008. 30952, 30956

Wenig, M., Spichtinger, N., Stohl, A., Held, G., Beirle, S., Wagner, T., Jähne, B., and Platt, U.:
Intercontinental transport of nitrogen oxide pollution plumes, *Atmos. Chem. Phys.*, 3, 387–
393, doi:10.5194/acp-3-387-2003, 2003. 30949, 30961, 30969

Whittaker, L. M. and Horn, L. H.: Northern Hemisphere extratropical cyclone activity for four
mid-season months, *J. Climatol.*, 4, 297–310, doi:10.1002/joc.3370040307, 1984. 30967

NO₂ long-range transport events in GOME-2 data

A. W. Zien et al.

[Title Page](#)
[Abstract](#)
[Introduction](#)
[Conclusions](#)
[References](#)
[Tables](#)
[Figures](#)
[Back](#)
[Close](#)
[Full Screen / Esc](#)
[Printer-friendly Version](#)
[Interactive Discussion](#)


Table 1. Properties of NO₂ plumes observed during long-range transport case studies as estimated from GOME-2 data and HYSPLIT backtrajectories. For all plumes, properties (except for plume age) are derived only from the observational data for the given date – no information from prior or later observations is used.

Date	Plume Center		Altitude [km]	Age [h]	NO ₂ content [GgN]	Area [10 ³ km ²]
North Atlantic						
17 Dec 2007	45° N	63° W	1.0	50	2.31	1093
18 Dec 2007	55° N	52° W	1.5	73	1.98	698
19 Dec 2007	58° N	42° W	2.0	95	0.65	207
South Africa						
9 Jul 2008	42° S	53° E	2.0	50	1.58	642
10 Jul 2008	41° S	78° E	1.5	73	1.74	1293
11 Jul 2008	35° S	93° E	6.0	96	1.40	1898
12 Jul 2008	30° S	103° E	4.5	119	0.39	881
Australia						
27 Apr 2008	46° S	159° E	4.0	47	1.83	1256
28 Apr 2008	60° S	175° W	1.0	69	0.89	311
29 Apr 2008	52° S	152° W	1.5	92	0.45	288
30 Apr 2008	43° S	141° W	3.0	115	0.16	319
Central Europe						
1 Oct 2010	60° N	0° W	1.0	21	0.38	372
2 Oct 2010	64° N	11° W	1.0	46	0.75	778

NO₂ long-range transport events in GOME-2 data

A. W. Zien et al.

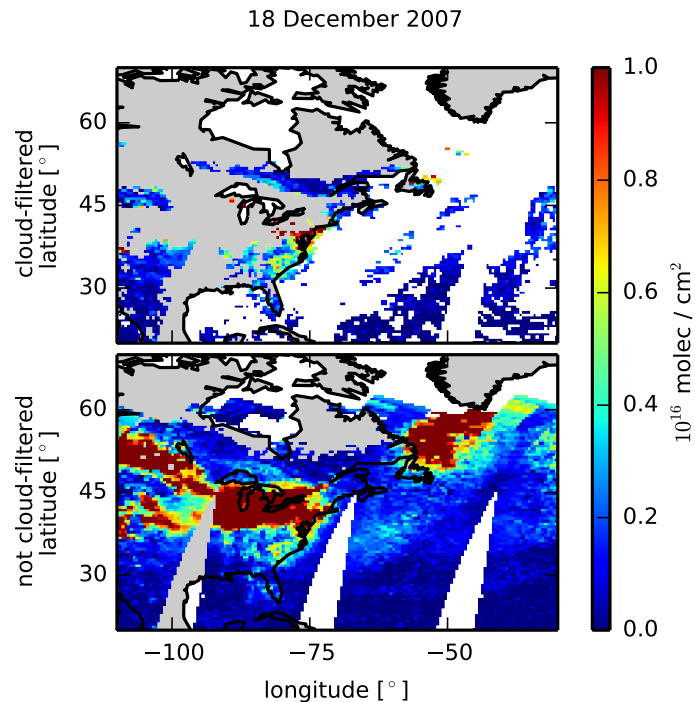


Fig. 1. GOME-2 tropospheric NO₂ vertical column density with (top) cloud-filtering enabled (FRESCO+ cloud fraction > 20%) and (bottom) disabled on 18 December 2007. A plume associated to a long-range transport event (following a cyclone) can be seen south of Greenland only in the non-filtered data.

NO₂ long-range transport events in GOME-2 data

A. W. Zien et al.

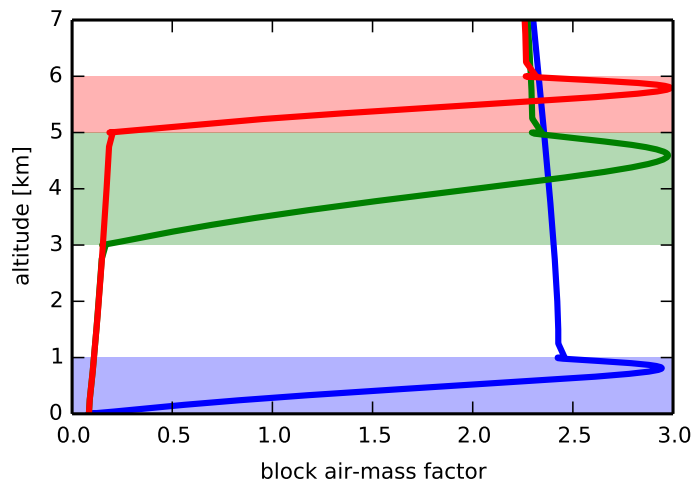


Fig. 2. Three exemplary block air-mass factors ($\lambda = 437.5$ nm) for scenes with clouds of optical thickness 20 at the respective shaded altitudes. Solar zenith angle and viewing angle are set to 0° , the surface albedo is set to $a = 0.1$. The absolute altitudes of trace gas and cloud only have a small impact on sensitivity – the dominant effect stems from the relation of their respective altitudes.

Title Page

Abstract

Introduction

Conclusions

References

Tables

Figures

◀

▶

◀

▶

Back

Close

Full Screen / Esc

Printer-friendly Version

Interactive Discussion



NO₂ long-range transport events in GOME-2 data

A. W. Zien et al.

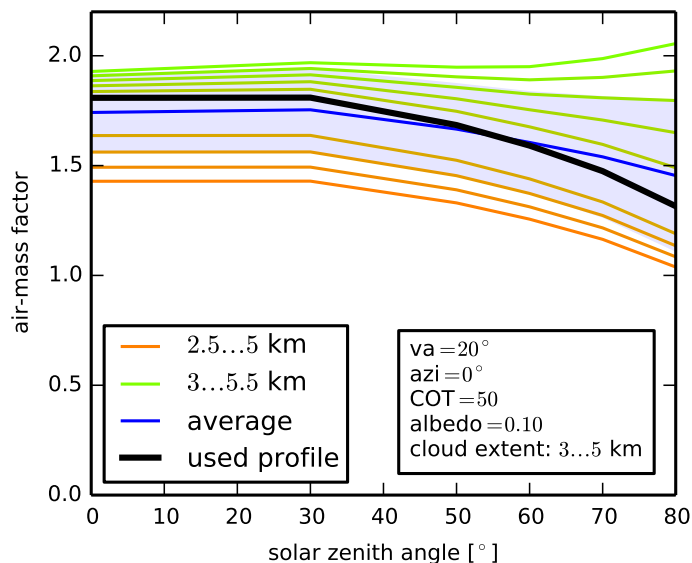


Fig. 3. Illustration of the air-mass factor dependency on the solar zenith angle for varying NO₂ profiles and an invariant cloud profile. The black line shows the profile used for this study. The ensemble average and the standard deviation are indicated in blue. We used a cloud vertical extent of 3...5 km, a surface albedo $a = 0.10$, a viewing angle $va = 20^\circ$, relative azimuth angle $azi = 0^\circ$ (forward direction) and cloud optical thickness $COT = 50$ (as used for data analysis).

Title Page

Abstract

Introduction

Conclusions

References

Tables

Figures

◀

▶

◀

▶

Back

Close

Full Screen / Esc

Printer-friendly Version

Interactive Discussion



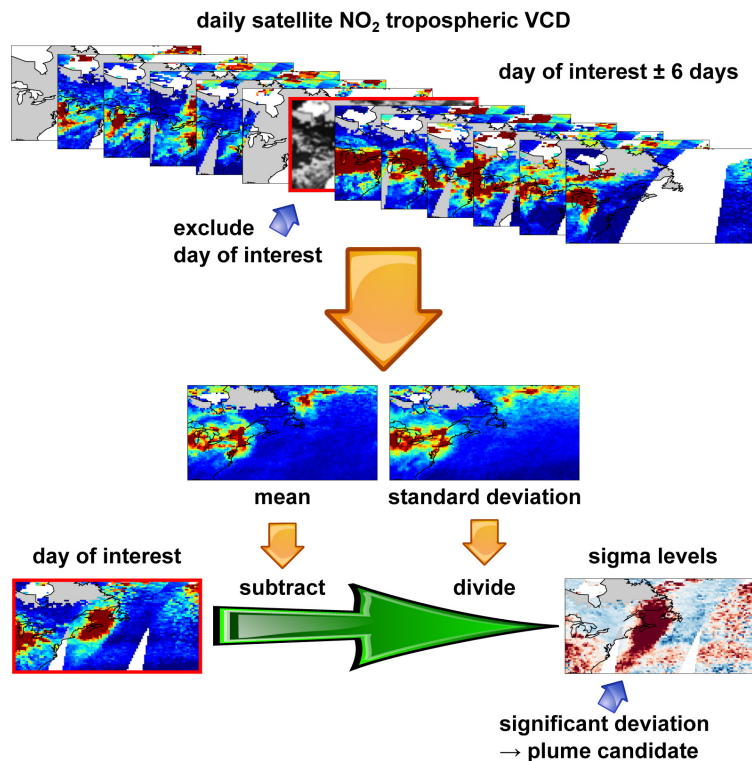


Fig. 4. Schematics of how long-range transport plumes are detected using our algorithm. The observational data are compared to a sliding mean and standard deviation of the six days preceding and following the day of observation. Strong positive anomalies in NO₂ vertical column densities are selected as candidates for long-range transport plumes.

Title Page	
Abstract	Introduction
Conclusions	References
Tables	Figures
◀	▶
◀	▶
Back	Close
Full Screen / Esc	
Printer-friendly Version	
Interactive Discussion	



NO₂ long-range transport events in GOME-2 data

A. W. Zien et al.

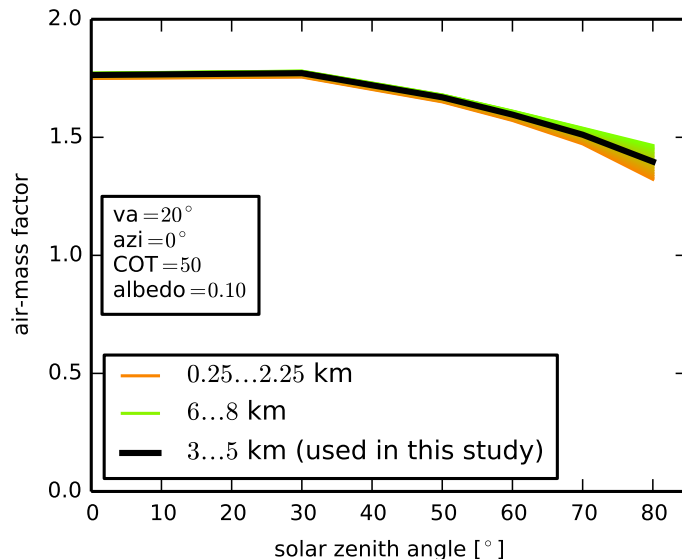


Fig. 5. Sample air-mass factor dependency on solar zenith angle for NO₂ fully mixed inside clouds at varying altitudes. The black line indicates the cloud and NO₂ profile used in this study. We used a surface albedo $a = 0.1$, a viewing angle $va = 20^\circ$, relative azimuth angle $azi = 0^\circ$ (forward direction) and cloud optical thickness $COT = 50$ (as was used for data analysis).

[Title Page](#)[Abstract](#)[Introduction](#)[Conclusions](#)[References](#)[Tables](#)[Figures](#)[◀](#)[▶](#)[◀](#)[▶](#)[Back](#)[Close](#)[Full Screen / Esc](#)[Printer-friendly Version](#)[Interactive Discussion](#)

NO₂ long-range transport events in GOME-2 data

A. W. Zien et al.

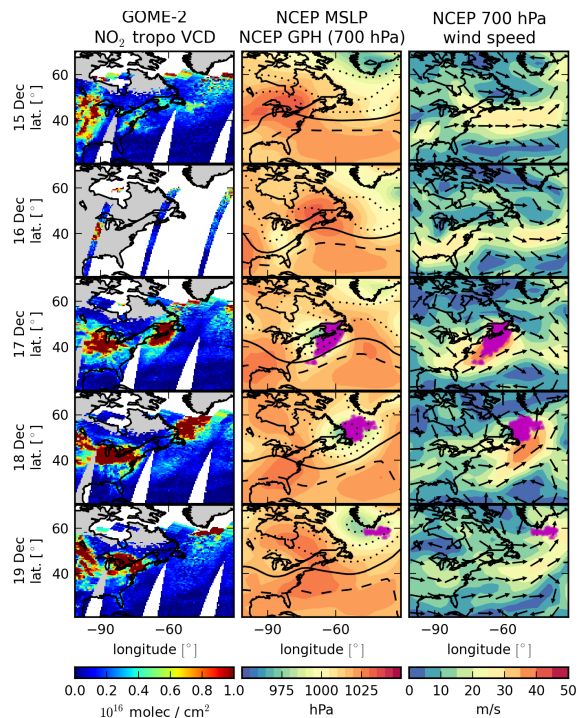


Fig. 6. Timeseries of the days preceding and during a long-range transport event over the North Atlantic on 17 to 19 December 2007. The locations of satellite pixels identified as belonging to the long-range transport plume are indicated by purple circles. Shown are (left) the GOME-2 NO₂ tropospheric vertical column density, (center) the NCEP DOE AMIP-II Reanalysis mean sea-level pressure (colors) and geopotential height at 700hPa (contours) and (right) horizontal wind speeds at 700hPa (amplitude and direction). For geopotential height, the solid line denotes 3km, dashed/dotted indicate higher/lower geopotential height in steps of 125m. A low pressure system is quickly evolving into a cyclone. It elevates an NO₂ plume – as seen in its backtrajectories – and transports it towards Greenland.

Title Page

Abstract

Introduction

Conclusions

References

Tables

Figures

◀

▶

◀

▶

Back

Close

Full Screen / Esc

Printer-friendly Version

Interactive Discussion



NO₂ long-range transport events in GOME-2 data

A. W. Zien et al.

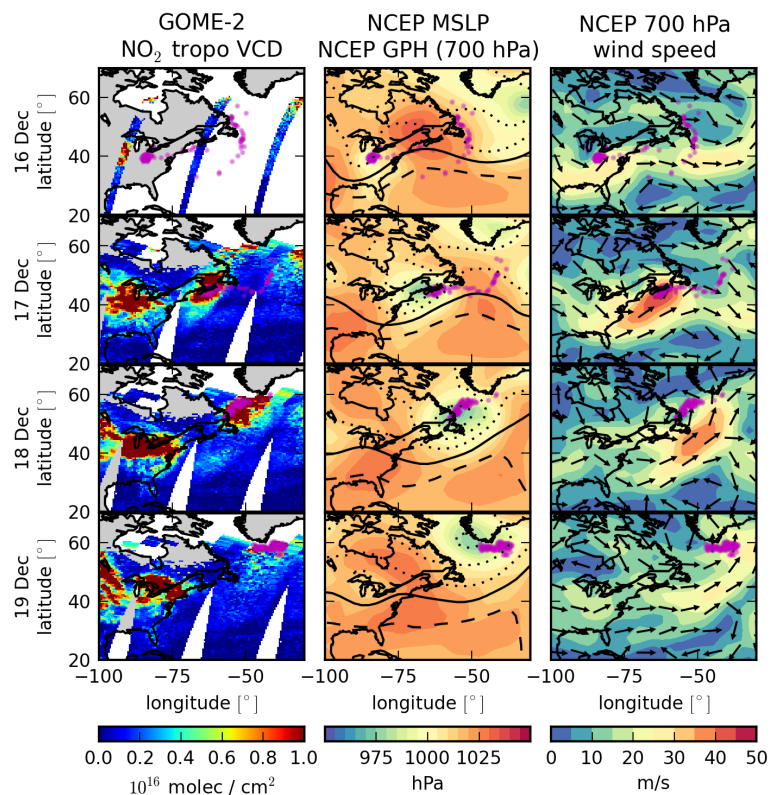


Fig. 7. Illustration of the backtrajectory of the last observation of this long-range transport event (19 December 2007). Data as in Fig. 6, but purple circles indicate the locations of the backtrajectories of the plume from 19 December 2007 at the respective dates. The plume detected on 19 December 2007 is only partially visible due to polar night. This becomes evident when comparing the backtrajectories on earlier dates with the observed NO₂ vertical column densities.

[Title Page](#)
[Abstract](#)
[Introduction](#)
[Conclusions](#)
[References](#)
[Tables](#)
[Figures](#)
[◀](#)
[▶](#)
[◀](#)
[▶](#)
[Back](#)
[Close](#)
[Full Screen / Esc](#)
[Printer-friendly Version](#)
[Interactive Discussion](#)


NO₂ long-range transport events in GOME-2 data

A. W. Zien et al.

Title Page

Abstract

Introduction

Conclusions

References

Tables

Figures

◀

▶

◀

▶

Back

Close

Full Screen / Esc

Printer-friendly Version

Interactive Discussion

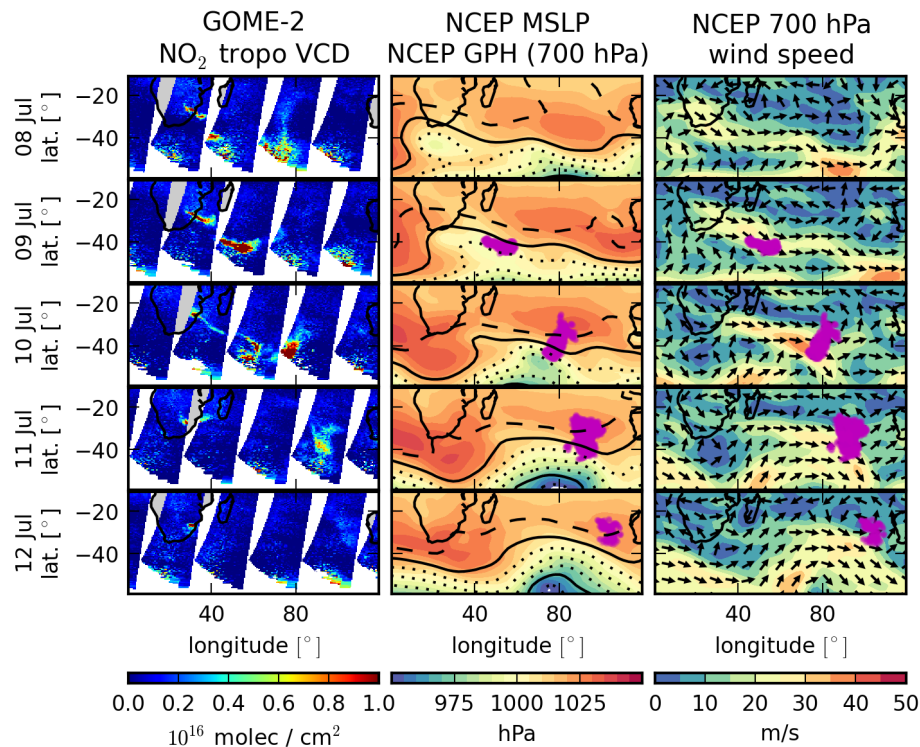


Fig. 8. As for Fig. 6, but showing a long-range transport event emitted from South Africa in July 2008. The NO₂ plume is transported from South Africa to the West Coast of Australia.

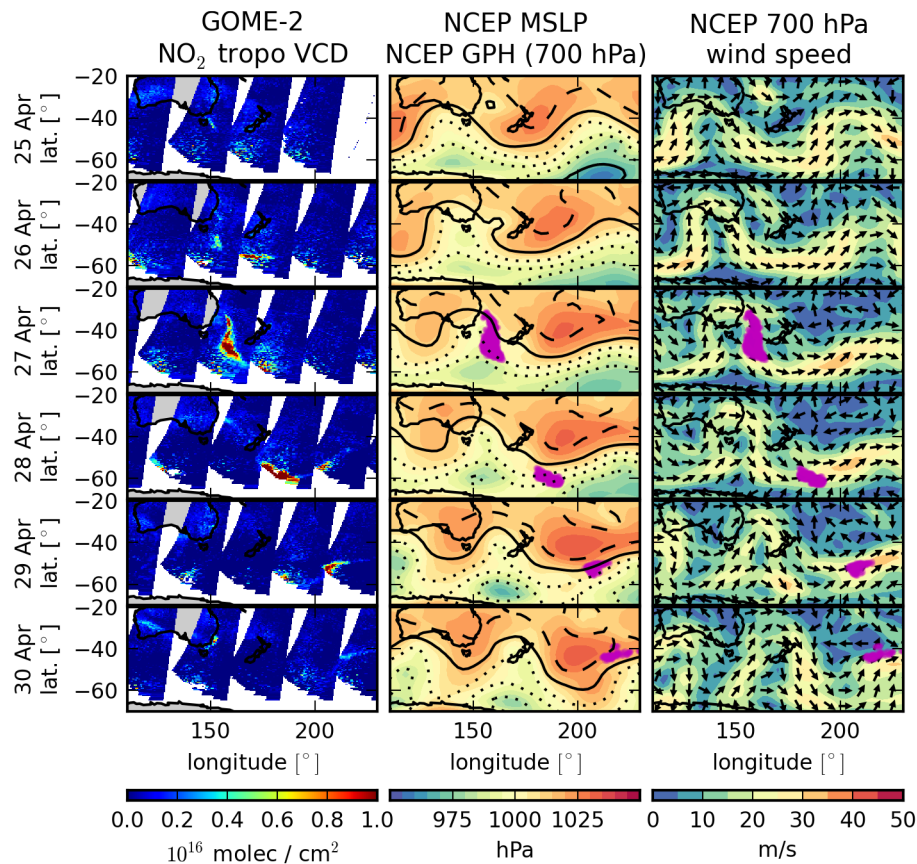


Fig. 9. As for Fig. 6, but showing a long-range transport event emitted in Australia in April 2008. The plume originates most likely from bush fires in Southwest Australia and follows the strong wind currents between highs over the Indian Ocean and lows over the Southern Ocean.

NO₂ long-range transport events in GOME-2 data

A. W. Zien et al.

Title Page

Abstract

Introduction

Conclusions

References

Tables

Figures

◀

▶

◀

▶

Back

Close

Full Screen / Esc

Printer-friendly Version

Interactive Discussion

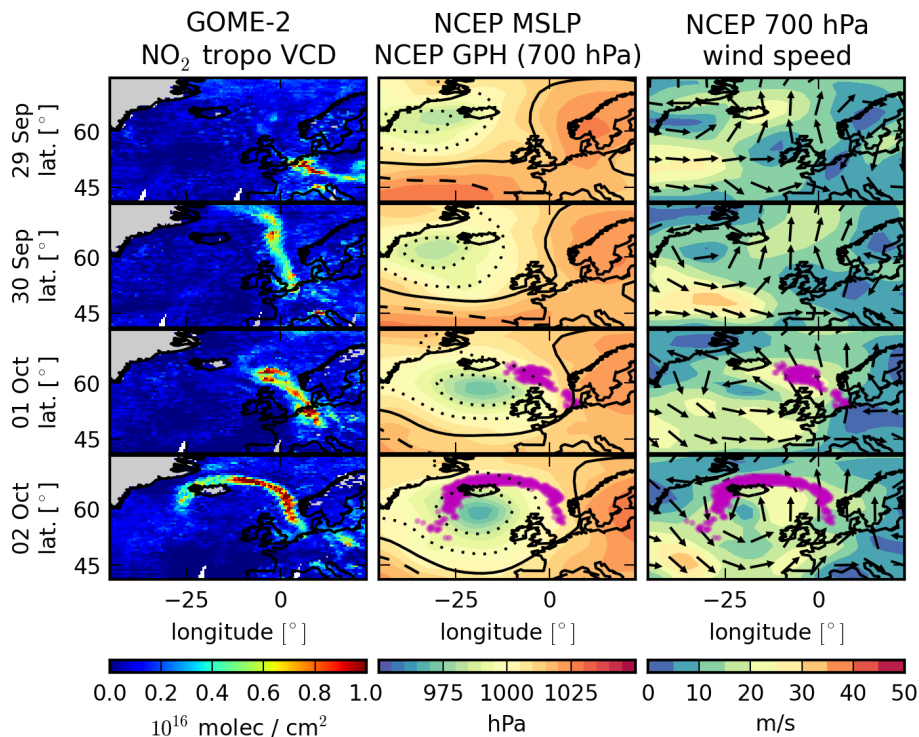


Fig. 10. As for Fig. 6, but showing a long-range transport event emitted in Europe in October 2010. The plume gets highly filamented when entering the cyclone. Note that the plume visible on 30 September 2010 separates from the rest of the plume and appears to have mostly been transported into the Arctic by 01 October 2010. Therefore, we do not include it in our analysis.

NO₂ long-range transport events in GOME-2 data

A. W. Zien et al.

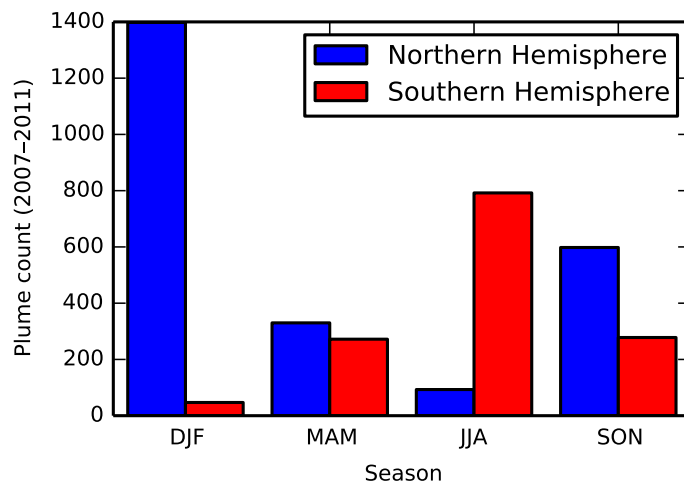


Fig. 11. Number of verified long-range transport plumes found by the detection algorithm in 2007–2011. There is a strong seasonality in both hemispheres, with a strong peak in local winter.

[Title Page](#)[Abstract](#)[Introduction](#)[Conclusions](#)[References](#)[Tables](#)[Figures](#)[◀](#)[▶](#)[◀](#)[▶](#)[Back](#)[Close](#)[Full Screen / Esc](#)[Printer-friendly Version](#)[Interactive Discussion](#)

NO₂ long-range transport events in GOME-2 data

A. W. Zien et al.

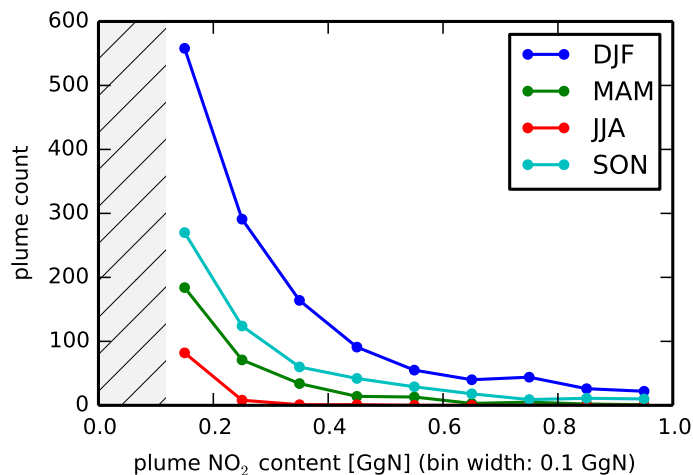


Fig. 12. NO₂ content of long-range transport events in the Northern Hemisphere, for different seasons. Note the lower mass limit of 5×10^{30} molecules (hatched area, corresponding to 0.12 GgN).

NO₂ long-range transport events in GOME-2 data

A. W. Zien et al.

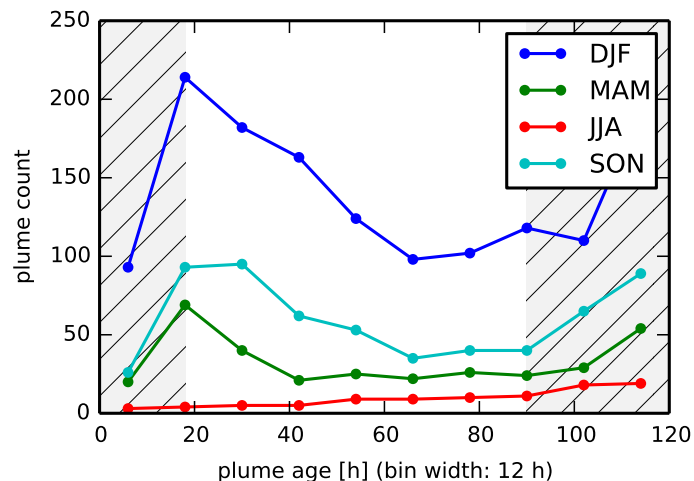


Fig. 13. Plume age at observation time of long-range transport events for 2007–2011, divided by season. The distribution illustrates the exponential decrease of long-range transport detections with age in the center. Two biases of the detection algorithm affect the hatched areas for low and high ages. See the text for details.

[Title Page](#)[Abstract](#)[Introduction](#)[Conclusions](#)[References](#)[Tables](#)[Figures](#)[⏪](#)[⏩](#)[◀](#)[▶](#)[Back](#)[Close](#)[Full Screen / Esc](#)[Printer-friendly Version](#)[Interactive Discussion](#)

NO₂ long-range transport events in GOME-2 data

A. W. Zien et al.

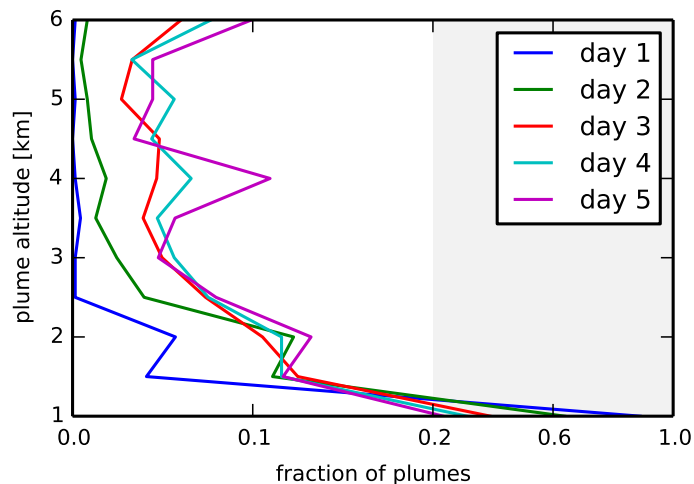


Fig. 14. Altitude distribution of NO₂ long-range transport plumes over the 11 altitude levels sampled in the HYSPLIT backtrajectories. Shown are the graphs for plumes younger than one day, between one and two days of age, etc. While most young plumes reside on the lowest level, they tend to distribute more equally in altitude over the following days. Note the compressed axis for fractions higher than 20%.

[Title Page](#)[Abstract](#)[Introduction](#)[Conclusions](#)[References](#)[Tables](#)[Figures](#)[◀](#)[▶](#)[◀](#)[▶](#)[Back](#)[Close](#)[Full Screen / Esc](#)[Printer-friendly Version](#)[Interactive Discussion](#)

NO₂ long-range transport events in GOME-2 data

A. W. Zien et al.

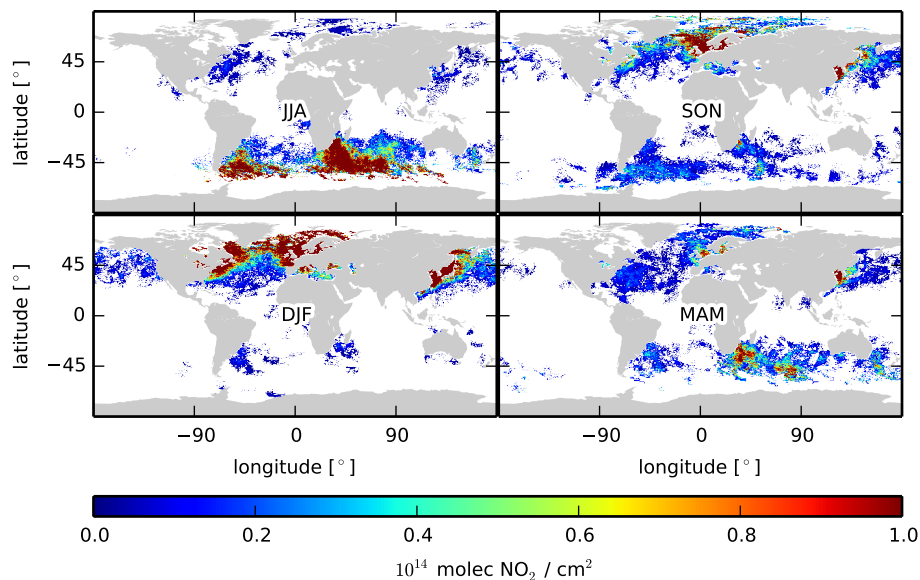


Fig. 15. Seasonal maps of the mean vertical column density of NO₂ observed in plumes associated to long-range transport events. Note that columns near Europe are always higher than columns near North America – at least partially due to its special geography.

[Title Page](#)[Abstract](#)[Introduction](#)[Conclusions](#)[References](#)[Tables](#)[Figures](#)[◀](#)[▶](#)[◀](#)[▶](#)[Back](#)[Close](#)[Full Screen / Esc](#)[Printer-friendly Version](#)[Interactive Discussion](#)

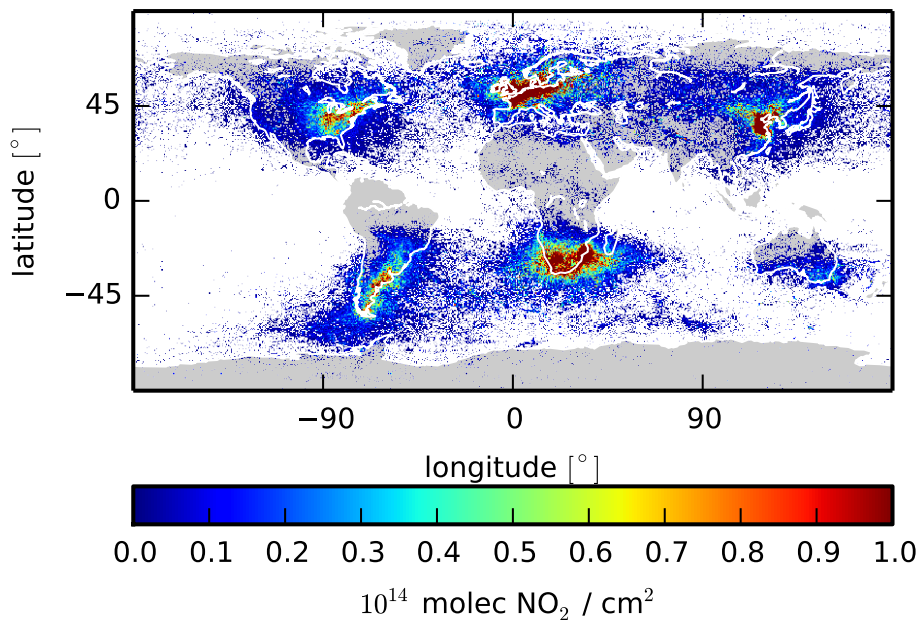


Fig. 16. Regional contribution to average NO_2 vertical column densities observed in long-range transport plumes. Sources of most long-range transport events are clearly visible. The high scatter originates from the low resolution of meteorological data used for the backtrajectories and uncertainties in the determination of the most likely backtrajectory.

NO_2 long-range transport events in GOME-2 data

A. W. Zien et al.

Title Page

Abstract

Introduction

Conclusions

References

Tables

Figures

◀

▶

◀

▶

Back

Close

Full Screen / Esc

Printer-friendly Version

Interactive Discussion



NO₂ long-range transport events in GOME-2 data

A. W. Zien et al.

Title Page

Abstract

Introduction

Conclusions

References

Tables

Figures

◀

▶

◀

▶

Back

Close

Full Screen / Esc

Printer-friendly Version

Interactive Discussion

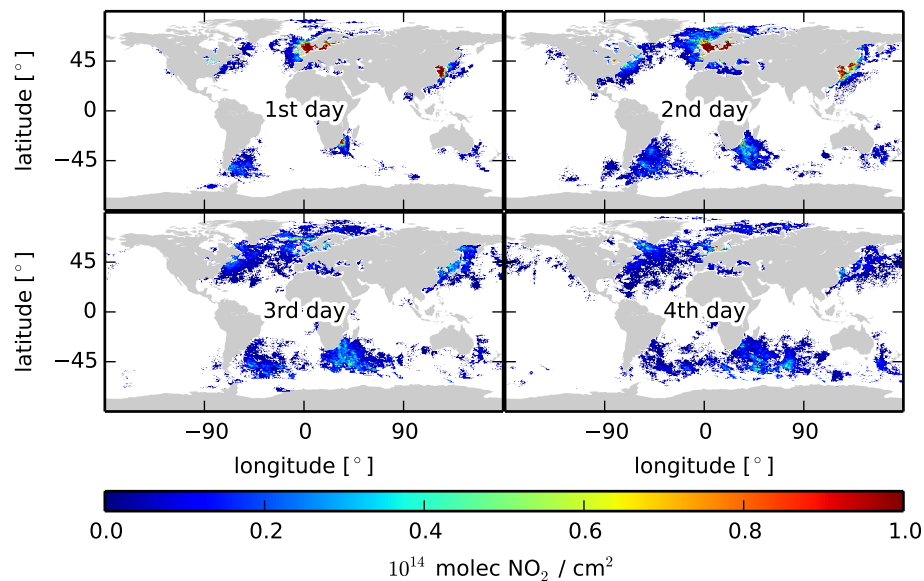


Fig. 17. Map of the mean NO₂ vertical column density observed in plumes of long-range transport events, binned by the age of plumes since emission at observation time.

NO₂ long-range transport events in GOME-2 data

A. W. Zien et al.

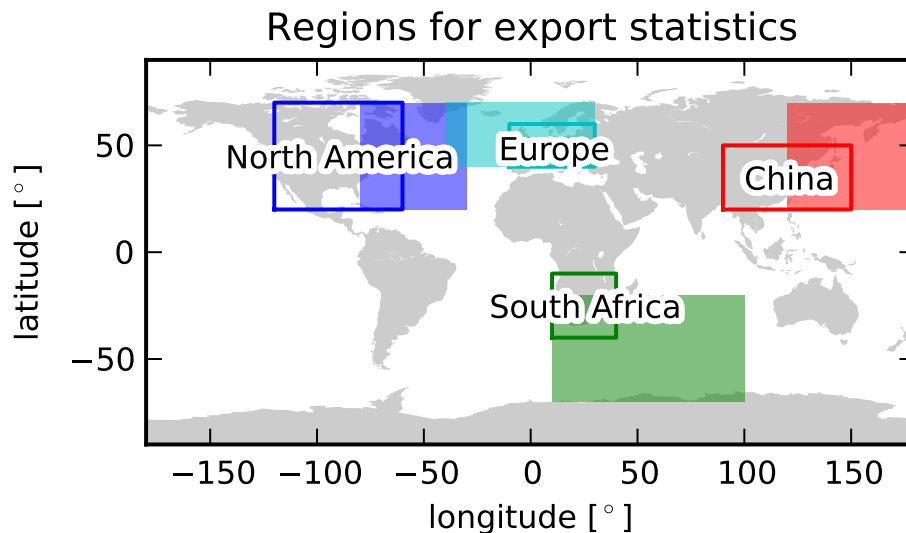


Fig. 18. The regions used for the statistical study. Only plumes are considered that were observed over the ocean in the filled rectangle and were found over land-masses in the open rectangle 24 h earlier.

[Title Page](#)[Abstract](#)[Introduction](#)[Conclusions](#)[References](#)[Tables](#)[Figures](#)[⏪](#)[⏩](#)[◀](#)[▶](#)[Back](#)[Close](#)[Full Screen / Esc](#)[Printer-friendly Version](#)[Interactive Discussion](#)

NO₂ long-range transport events in GOME-2 data

A. W. Zien et al.

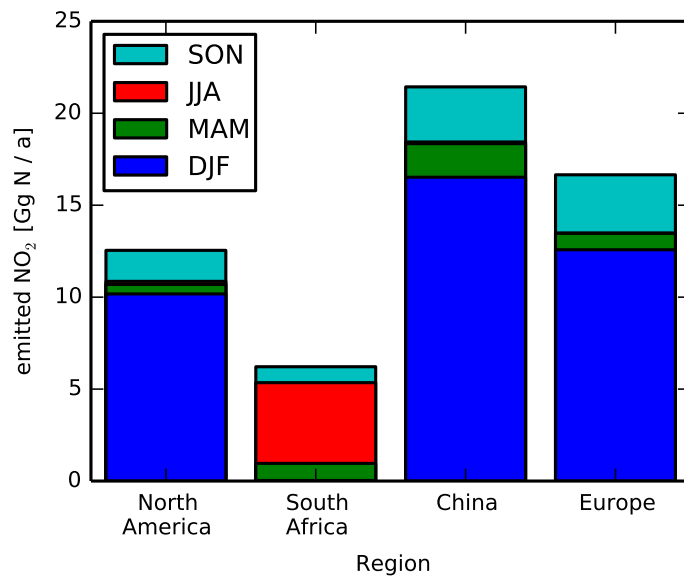


Fig. 19. Total yearly NO₂ content in long-range transport plumes emitted in the regions shown in Fig. 18 for different seasons.

NO₂ long-range transport events in GOME-2 data

A. W. Zien et al.

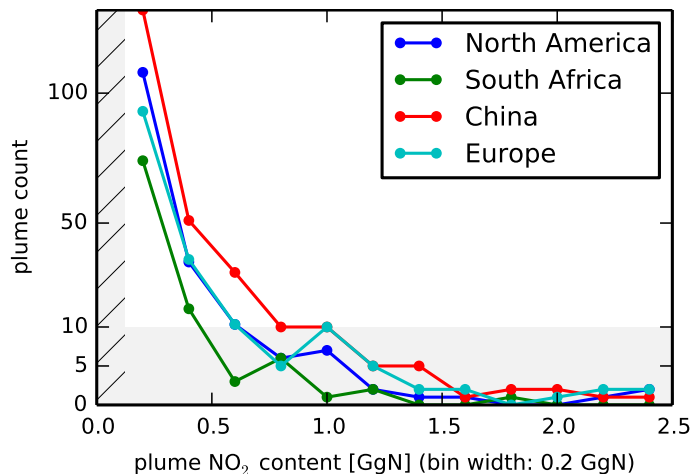


Fig. 20. NO₂ content distribution of long-range transport events observed in the respective regions. South Africa has the smallest plumes, while Europe emits a large fraction of NO₂-rich plumes. The data are binned in steps of 0.2 GgN. The hatched area denotes the NO₂ content below which plumes are not included in the analysis. The shaded area indicates a stretched axis to illustrate the frequency of plumes with high NO₂ content.

Title Page

Abstract

Introduction

Conclusions

References

Tables

Figures

◀

▶

◀

▶

Back

Close

Full Screen / Esc

Printer-friendly Version

Interactive Discussion



NO₂ long-range transport events in GOME-2 data

A. W. Zien et al.

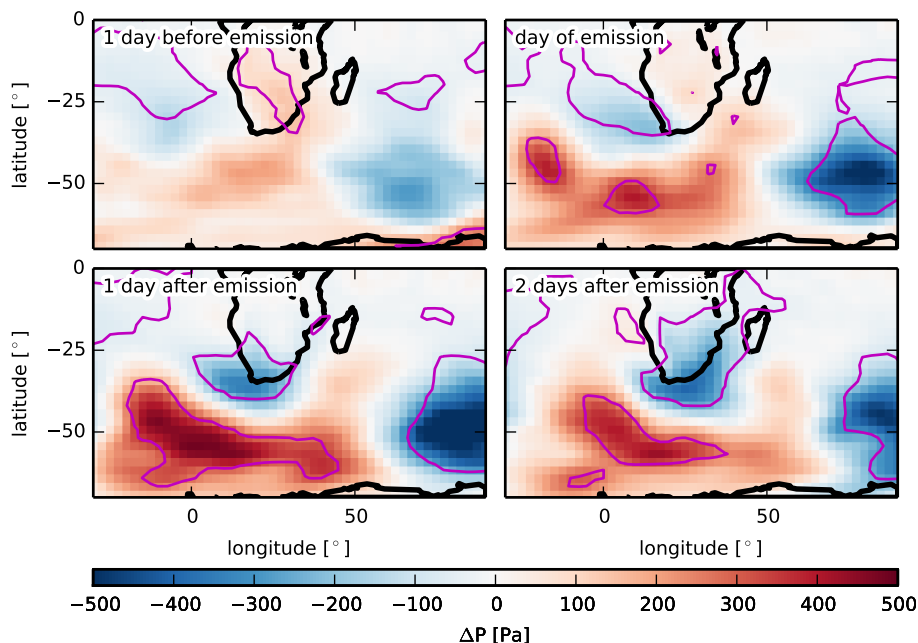


Fig. 21. NCEP DOE AMIP-II Reanalysis mean sea-level pressure anomaly (given in Pa) for the days of plume emission in the South African region. Only events in JJA (2007–2011) are shown, to prevent biases from meteorologic seasonality. 99%-significance contours from the Mann–Whitney U test are depicted in magenta. The image shows significant high and low pressure patterns in the southern midlatitudes, moving from West to East.

Title Page

Abstract

Introduction

Conclusions

References

Tables

Figures

◀

▶

◀

▶

Back

Close

Full Screen / Esc

Printer-friendly Version

Interactive Discussion



NO₂ long-range transport events in GOME-2 data

A. W. Zien et al.

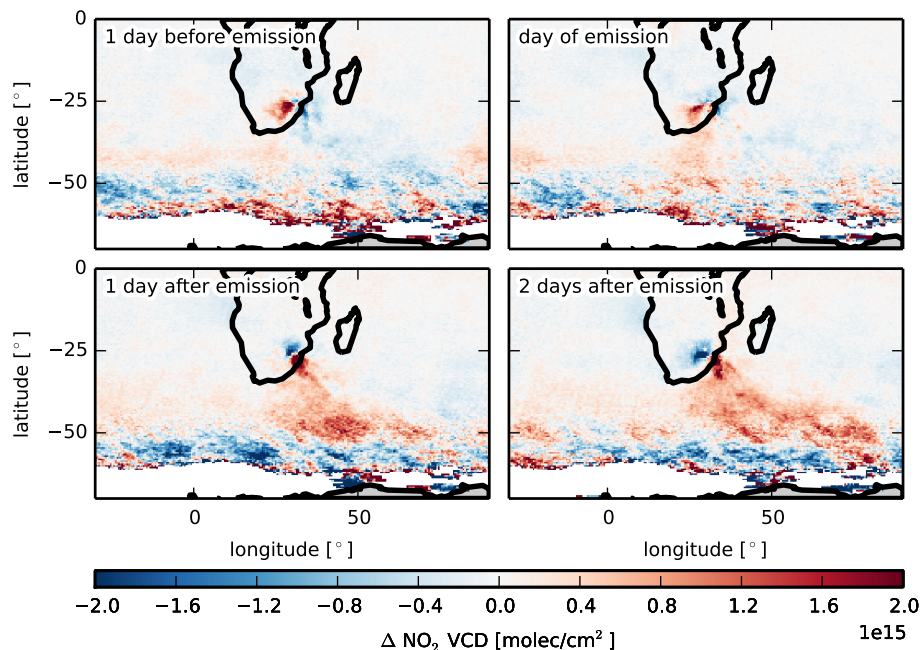


Fig. 22. As in Fig. 21, but showing anomalies in GOME-2 NO₂ vertical column densities. There is an anomaly towards high values over the Highveld region before plume emission, moving to the South-East during the long-range transport event. After emission, the NO₂ vertical column densities over the Highveld region are on average lower. High fluctuations in the GOME-2 data result in visible noise in the anomalies.

Title Page

Abstract

Introduction

Conclusions

References

Tables

Figures

◀

▶

◀

▶

Back

Close

Full Screen / Esc

Printer-friendly Version

Interactive Discussion



NO₂ long-range transport events in GOME-2 data

A. W. Zien et al.

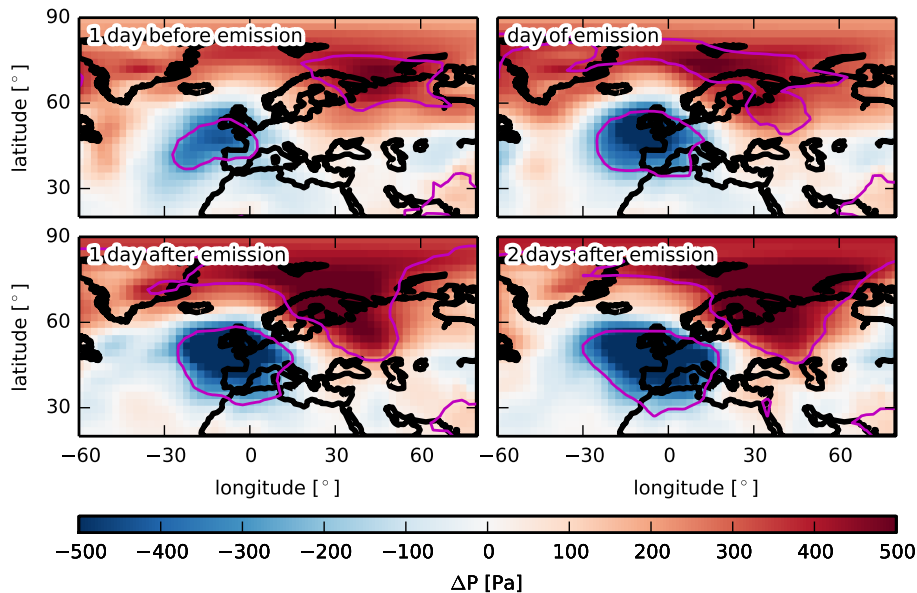


Fig. 23. As in Fig. 21, but for the Central European region. Only events in DJF (2007–2011) are shown. The image shows significant stationary high and low pressure patterns in the Arctic and over Europe.

[Title Page](#)[Abstract](#)[Introduction](#)[Conclusions](#)[References](#)[Tables](#)[Figures](#)[◀](#)[▶](#)[◀](#)[▶](#)[Back](#)[Close](#)[Full Screen / Esc](#)[Printer-friendly Version](#)[Interactive Discussion](#)